

**1 Long-lived meso-scale eddies in the Eastern**  
**2 Mediterranean Sea: analysis of 20 years of AVISO**  
**3 geostrophic velocities.**

4 

---

Nadia Mkhinini,<sup>1,2</sup> Andre Louis Santi Coimbra,<sup>2</sup> Alexandre Stegner,<sup>1,2</sup>  
Thomas Arsouze,<sup>1,2,\*</sup> Isabelle Taupier-Letage,<sup>3</sup> and Karine Béranger,<sup>2</sup>

---

\*Corresponding author: Thomas Arsouze, Laboratoire de Météorologie Dynamique, École Polytechnique, 91125 Palaiseau Cedex, France (thomas.arsouze@ensta-paristech.fr)

<sup>1</sup>Laboratoire de Météorologie Dynamique,  
École Polytechnique, Palaiseau, France

<sup>2</sup>UME, ENSTA-ParisTech, 828 Boulevard  
des Marchaux, 91762 Palaiseau Cedex,  
France

<sup>3</sup>Aix Marseille Université, CNRS,  
Université de Toulon, IRD, MIO UM 110,  
13288, Marseille, France

5 **Abstract.** We analyzed 20 years of AVISO data set to detect and char-  
6 acterize long-lived eddies, which stay coherent more than six months, in the  
7 Eastern Mediterranean Sea. In order to process the coarse gridded ( $1/8^\circ$ ) AVISO  
8 geostrophic velocity fields, we optimized a geometrical eddy detection algo-  
9 rithm. Our main contribution was to implement a new procedure based on  
10 the computation of the Local and Normalized Angular Momentum (LNAM)  
11 to identify the positions of the eddy centers and to follow their Lagrangian  
12 trajectories. We verify on two meso-scale anticyclones, sampled during the  
13 EGYPT campaign in 2006, that our methodology provides a correct estima-  
14 tion of the eddy centers and their characteristic radius corresponding to the  
15 maximal tangential velocity. Our analysis reveals the dominance of anticy-  
16 clones among the long-lived eddies. This cyclone-anticyclone asymmetry ap-  
17 pears to be much more pronounced in Eastern Mediterranean Sea than in  
18 the global ocean. Then we focus our study on the formation areas of long-  
19 lived eddies. We confirm that the generations of the Ierapetra and the Pelops  
20 anticyclones are recurrent and correlated to the Etesian wind-forcing. We  
21 also provide some evidence that the smaller cyclonic eddies formed at the  
22 southwest of Crete may also be induced by the same wind forcing. On the  
23 other hand, the generation of long-lived eddies along the Libyo-Egyptian coast  
24 are not correlated to the local wind-stress curl but surprisingly, their ini-  
25 tial formation points follow the Herodotus Trough bathymetry. Moreover,  
26 we identify a new formation area, not discussed before, along the curved shelf  
27 off Benghazi.

## 1. Introduction

28 The improved spatial resolution of sea surface fields in the AVISO altimetry merged  
29 data revealed the prevalence of meso scale eddies throughout most of the oceans [*Isern-*  
30 *Fontanet et al.*, 2003, 2006b; *Morrow et al.*, 2004; *Chelton et al.*, 2007, 2011; *Chaigneau*  
31 *et al.*, 2008, 2009]. Among the various methods used to detect and sample surface oceanic  
32 eddies from field measurements, the use of sea surface altimetry, which is not affected  
33 by cloud coverage, is among the most efficient ways to track long-lived eddies. The  
34 recent progress in automated eddy detection algorithms [*Sadarjoen et al.*, 1998; *Isern-*  
35 *Fontanet et al.*, 2003; *Nencioli et al.*, 2010; *Chelton et al.*, 2011] enables to identify the  
36 positions of coherent structures and to follow their Lagrangian trajectories during several  
37 months. Among the thousands eddies that could be identified at any given time a small  
38 but significant number of long-lived eddies, lasting more than six months, were detected  
39 in specific regions such as the southeastern Atlantic Ocean [*Schonten et al.*, 2000], the  
40 eastern South-Pacific [*Chaigneau et al.*, 2008] or the northeastern subtropical Atlantic  
41 [*Sangrà et al.*, 2009]. Moreover, *Chelton et al.* [2011] detected, over 16 years of data record  
42 of the global ocean, more than 600 surface eddies with lifetime that exceed two years.  
43 The presence of such long-lived eddies could strongly impact the surface circulation at  
44 both local and regional scale. Indeed, these coherent structures trap and transport heat,  
45 mass, momentum, and biogeochemical properties from their regions of formation to remote  
46 areas.

47 In many closed or semi-closed seas the circulation is dominated by gyres and coastal  
48 eddies and the kinetic energy of the instantaneous eddy field is larger than the kinetic en-

49 ergy of the long-term average circulation. This is the case of the Mediterranean sea which  
50 exhibits a complex circulation system [*Millot and Taupier-Letage, 2005; Isern-Fontanet*  
51 *et al., 2006; Sorgente et al., 2011; Menna et al., 2012*]. The excess of evaporation in the  
52 Mediterranean sea is mainly compensated by the entrance of fresh Atlantic waters (AW)  
53 through the Strait of Gibraltar. Part of this AW crosses the Sicilian channel and drives  
54 the surface circulation of the eastern Mediterranean Sea, i.e. the Ionian and Levantine  
55 sub-basin (Fig.1a). As expected for a density-driven surface current, the light AW in-  
56 duces a mean cyclonic circulation in the closed basin. The twenty year average of the  
57 AVISO surface geostrophic velocities (Fig.1b) exhibit a mean eastward flow along the  
58 Libyo-Egyptian coast and a mean westward flow south of Crete. However, such temporal  
59 averaging smooth out the spatio-temporal variability of coherent structures and therefore  
60 oversimplified the basin circulation. As pointed out by *Isern-Fontanet et al. [2006]* a large  
61 number of studies on the mediteranean circulation are focused on mean Eulerian statistics  
62 or long-term averaged circulation [*Robinson et al., 1991; Larnicol et al., 2002; Rio et al.,*  
63 *2007; Poulain et al., 2012; Menna et al., 2012*] rather than on the formation and the tra-  
64 jectories of coherent and long-lived vortices. Indeed, the instabilities of the surface flow,  
65 the interactions with the complex bathymetry (Fig. 1a) and the local wind stress generate  
66 numerous vortices in several parts of the basin. Hence, the surface circulation exhibit a  
67 strong spatio-temporal variability induced by a turbulent eddy field or highly variable  
68 currents. This is especially true in the eastern basin where the unsteady path of the AW  
69 is under debate [*Millot and Taupier-Letage, 2005; Gerin et al., 2009; Millot and Gerin,*  
70 *2010*] and the mechanism of formation of coherent eddies along the Libyo-Egyptian coast

71 poorly known. Our study focuses on the sub-basin area [17°E - 30°E, 30°N - 36.3°N], the  
72 black rectangle in Fig.1a, where in-situ measurements are scarce.

73 Several long-lived meso scale features have been pointed out by observations in the east-  
74 ern Mediterranean Sea [*Pinardi et al.*, 2003]. Two well documented eddies, the Ierapetra  
75 (IE) and the Pelops (PE) anticyclones which are respectively located at the northwest  
76 and the southwest corner of Crete [*Theocharis et al.*, 1993; *Matteoda and Glenn*, 1996]  
77 are recurrently generated in summer. Some large-scale anticyclonic gyres are visible, in  
78 these areas, on the long-term average of the surface circulation (Fig.1b). However, these  
79 eddies are not steady or permanent features even if they were observed during several  
80 months and could sometimes survive more than a year. For instance, during the fall 1997  
81 an old IE merged with a new IE leading to a robust anticyclonic eddy which trapped the  
82 summertime warm water in its core for almost two years [*Hamad et al.*, 2006]. Other  
83 meso scale anticyclones such as one Lybio-Egyptian eddy (called LE) [*Hamad et al.*, 2006;  
84 *Sutyryn et al.*, 2009] or the Mesra-Matruh eddies [*Hamad et al.*, 2006; *Gerin et al.*, 2009;  
85 *Amitai et al.*, 2010; *Menna et al.*, 2012] were documented from surface observation or  
86 in-situ measurements in the area. However, both their life time and their formation areas  
87 remain unclear. Besides, the recurrent or the sporadic nature of the various meso scale  
88 anticyclones, who are detected in this area, are still under discussion.

89 The main goals of this work are to identify the sub-regions where long-lived eddies  
90 are generated recurrently in the eastern Mediterranean sea, to characterize their size and  
91 intensity, and to follow their trajectories. In the present paper, our study focuses on  
92 coastal eddies (i.e. generated close to the shelf) which are able to trap and transport  
93 coastal waters in the center of the basin of the eastern Mediterranean Sea and to impact

94 significantly the sub-basin circulation in the [17°E - 30°E, 30°N - 36.3°N] area. We use  
 95 the geostrophic velocities derived from the absolute dynamical topography of the 20-year  
 96 AVISO data set covering the period 1993 to 2012. In order to efficiently detect and follow  
 97 long-lived eddies using this relatively coarse resolution data set we adapt and optimized  
 98 the geometrical algorithm of *Nencioli et al.* [2010]. The optimized algorithm is detailed  
 99 and the accuracy of our method is tested through an intercomparison of this optimized  
 100 algorithm with few in-situ measurements in section 2. A twenty-year climatology of long-  
 101 lived coastal eddies in the eastern Mediterranean Sea is then presented in section 3. We  
 102 performed here a thorough analysis of the cyclone-anticyclone asymmetry. We identify  
 103 the main formation areas of long-lived eddies, we study their seasonal variability and  
 104 suggest possible formation mechanisms. Finally, in section 4, we discuss these results and  
 105 their impacts on the sub-basin circulation.

## 2. Optimized algorithm for detection of coastal eddies

106 In order to characterize the eddy field, we chose to use the surface velocity instead  
 107 of the sea surface height for several reasons. The first one is that the main dynamical  
 108 properties of surface intensified vortices, namely their drifting speed [*Stegner and Zeitlin,*  
 109 1996; *Sutyryn et al., 2009*] and their stability characteristics [*Stegner and Dritschel, 2000;*  
 110 *Teinturier et al., 2010; Lazar et al., 2013a, b*], are driven by the vortex Rossby number  
 111  $Ro = V_{max}/(f R_{max})$  and the Burger number  $Bu = (R_d/R_{max})^2$ , where  $V_{max}$  is the maxi-  
 112 mal azimuthal velocity,  $R_{max}$  the corresponding radius,  $R_d$  the internal deformation radius  
 113 and  $f$  the Coriolis parameter. Therefore, working directly with the velocities provides a  
 114 direct quantification of the Rossby number  $Ro$ . Besides, in order to quantify accurately  
 115 the eddy size and therefore the Burger number  $Bu$ , the radius  $R_{max}$  corresponding to

116 the maximum tangential velocity is a simple and well defined length. Moreover, the ac-  
117 curate quantification of the vortex size  $R_{max}$  and intensity  $V_{max}$  from the velocity field,  
118 provided by the AVISO data set or numerical models, will allow a direct comparison with  
119 in-situ measurements such as ADCP transects or surface velocities derived from drifters  
120 trajectories.

121 Among the wide variety of identification methods based on the velocity field [*Sadarjoen*  
122 *et al.*, 1998; *Isern-Fontanet et al.*, 2003; *Nencioli et al.*, 2010] we chose to use the approach  
123 proposed by *Nencioli et al.* [2010] which identify, for every center of rotation detected,  
124 a closed streamline corresponding to the maximal velocity ring. However, when we first  
125 applied this algorithm to the geostrophic velocities provided by AVISO (with an optimal  
126 tuning of the parameters) we were able to detect only a low number of meso scale eddies.  
127 Hence, in order to improve the eddy detection and the eddy tracking it was needed to  
128 significantly modify the initial algorithm. We detail below the characteristics of the data  
129 set, the main optimizations we performed on the algorithm and the comparisons of this  
130 optimized method with in-situ drifters and SST patterns.

## 2.1. AVISO geostrophic velocities

131 The domain of the present study corresponds to a large fraction of the eastern  
132 mediterranean basin, between the meridians of 17°E and 30°E and the parallels of 30°N  
133 and 37°N. For this region we used the geostrophic velocity fields provided by AVISO  
134 (<http://www.aviso.oceanobs.com>) which are derived from the Absolute Dynamical To-  
135 pography (ADT). The distributed regional product combines, for the years 1993– 2012,  
136 satellite altimetry data from the Topex/ Poseidon, ERS, Jason–1, and Envisat missions.  
137 This merged satellite product is projected on a 1/8° horizontal resolution Mercator grid,

138 in time intervals of 7 days. This horizontal resolution is, in the Mediterranean sea, at the  
139 order of the internal deformation radius ( $R_d = 10 - 12\text{km}$ ). Hence, only large meso scale  
140 eddies, with a typical radius  $R_{max}$  larger than the deformation radius, could be identified  
141 from this data set. Besides, the accuracy of the eddy center identification could be affected  
142 by the limited numbers of vectors in the vortex core (AVISO  $1/8^\circ$  resolution).

## 2.2. Optimized algorithm for the detection of coastal eddies

### 143 2.2.1. Angular momentum method for eddy center detection

144 The first step of the method proposed by *Nencioli et al.* [2010] is to identify the centers  
145 of rotation in the velocity field. The algorithm looks for all pairs of points in the domain  
146 where there is a zonal and meridional velocity shear. At that stage, too many couple of  
147 points are selected and most of them should be excluded. Hence, the algorithm of *Nencioli*  
148 *et al.* [2010] searches for the local velocity minimum inside a small square domain centered  
149 on the selected points. However the search for a velocity minima, may lead to systematic  
150 detection errors when hyperbolic and elliptic points of the velocity field are too close to  
151 each other. Such configuration is shown in 2a. In this case, two vortices are next to  
152 each other and the algorithm will select the velocity minima at the hyperbolic point  $H$  of  
153 intersection between the two vortices instead of the two grid points  $E_1$  and  $E_2$  which are  
154 close to the vortex centers (elliptical points). Similar configuration occurs when a coastal  
155 current form a large meander and a vortex is detached. When the current meander starts  
156 to have a close streamline the elliptical point (i.e. the vortex center) will also be very  
157 close to the hyperbolic point.

158 To correct this problem and optimize the automatic eddy detection, we totally changed  
159 the second procedure. Instead of searching for a velocity minima, a local quantity sensi-

160 tive to the velocity errors at the grid scale, we decided to quantify an integral quantity  
 161 proportional to the local angular momentum. For each grid point  $X_i$ , we quantify a Local  
 162 and Normalized Angular Momentum ( $LNAM$ ) according to the formula:

$$LNAM(X_i) = \frac{\sum_j \underline{X_i X_j} \times \underline{V_j}}{\sum_j \underline{X_i X_j} \cdot \underline{V_j} + \sum_j |\underline{X_i X_j}| |\underline{V_j}|} = \frac{L_i}{S_i + BL_i} \quad (1)$$

163 where  $X_j$  and  $\underline{V_j}$  are respectively the position and the velocity vector of a grid point  
 164 neighbor of  $X_i$ . The sum is made over the  $n \times n$  neighbors points, inside a square domain  
 165 centered on  $X_i$ . We chose here a typical size  $n = 5$ . This  $LNAM$  parameter is propor-  
 166 tional to the local angular momentum  $L_i = \sum_j \underline{X_i X_j} \times \underline{V_j}$  at the grid point  $X_i$  and it is  
 167 renormalized by  $BL_i = \sum_j |\underline{X_i X_j}| |\underline{V_j}|$  an upper bound for the angular momentum (i.e.  
 168  $-BL_i \leq L_i \leq BL_i$ ). Besides, we add  $S_i = \sum_j \underline{X_i X_j} \cdot \underline{V_j}$  in the renormalization term. The  
 169 sum of the scalar products  $S_i$  will reach a large value for hyperbolic points and be equal  
 170 to zero for elliptical points. For a symmetric vortex if  $X_i$  is the vortex center,  $S_i = 0$  and  
 171 the  $LNAM$  parameter will reach an extremal value 1 ( $-1$ ) for a cyclonic (anticyclonic)  
 172 eddy. Hence, this parameter does not depend on the vortex intensity and is build to make  
 173 a net distinction between hyperbolic and elliptical points. According to the Fig.2b, when  
 174 this new  $LNAM$  parameter is used to detect the eddy centers on the same velocity field as  
 175 in Fig.2a only the two elliptical points  $E_1$  and  $E_2$  are identified. Nevertheless, this param-  
 176 eter will also select the centers of current meanders even if there is no closed streamlines,  
 177 in other words the extrema of the  $LNAM$  parameter do not guarantee a coherent eddy  
 178 structure able to trap water masses in its core. Hence, we need to add a third validation  
 179 step. We chose to keep the selected centers if we can find at least one closed streamline  
 180 in its vicinity. The streamlines calculations are detailed below.

### 181 2.2.2. Eddy size and intensity

182 In order to define the eddy size and its intensity we used, as *Nencioli et al.* [2010], the  
 183 contours lines of the streamfunction field. Once the possible locations of vortex centers are  
 184 identified the local streamfunction is computed around each selected point. An iterative  
 185 process select an increasing set of rectangular domain until a closed streamline having  
 186 the highest mean velocity  $V_{max}$  (averaged along the streamline) is found. This closed  
 187 streamline is registered as the characteristic vortex contour. Inside this contour, the  
 188 velocity magnitude increases radially from the vortex center. The eddy radius is then  
 189 defined as the equivalent radius of a circle with the same area  $A$  as the one delimited by  
 190 the closed characteristic contour:

$$R_{max} = \sqrt{\frac{A}{\pi}} \quad (2)$$

191 This procedure quantifies precisely for every detected eddy a characteristic size  $R_{max}$   
 192 and intensity  $V_{max}$ . Then, we can directly compute the vortex Rossby number  $Ro =$   
 193  $V_{max}/(f R_{max})$  and the Burger number  $Bu = (R_d/R_{max})^2$ . At that stage we also interpo-  
 194 late the characteristic vortex contour by an ellipse and estimate an equivalent ellipticity  
 195  $\epsilon = 1 - \frac{b}{a}$  (also called the flattening parameter) where  $b$  is the semi- minor axis and  $a$   
 196 is the semi- major axis. The ellipticity of the characteristic contour could then be used  
 197 to remove highly distorted structures in statistical analysis. Moreover, we ignored eddies  
 198 with a radius  $R_{max}$  smaller than  $15km$ . In fact, real eddies smaller than this threshold  
 199 are not correctly resolved in the AVISO grid.

200 Fig.3 shows the 27 eddies detected by this optimized algorithm from the geostrophic  
 201 velocity field (AVISO ADT data set) for the week 20 – 27 September 2006 in the domain

202 under study. The eddy centers identified by the *LNAM* field are marked with a black star  
203 and the solid lines (dashed lines) correspond to the characteristic vortex contours plotted  
204 for each anticyclones (cyclones).

205 The comparison with the widely used eddy detection algorithm based on the Okubo-  
206 Weiss (OW) parameter [*Isern-Fontanet et al.*, 2003, 2004, 2006; *Morrow et al.*, 2004;  
207 *Chelton et al.*, 2007] is given in appendix A. The OW method, applied on the same  
208 surface velocity field, induces a strong excess of detection. More than 55 eddies were  
209 detected (Fig.18) in comparison to the 27 eddies identified with our optimized algorithm  
210 (Fig.3). This systematic over detection induced by the OW method was also highlighted  
211 in the previous studies [*Isern-Fontanet et al.*, 2006; *Chaigneau et al.*, 2008; *Nencioli et al.*,  
212 2010]. Specific filters could be used to reduce the small-scale noise and the number of  
213 eddy detected [*Chelton et al.*, 2007; *Souza et al.*, 2011] but nevertheless, unlike the *LNAM*  
214 parameter we used, the OW method is highly sensitive to the variance of the flow field  
215 and therefore the threshold parameter.

### 216 **2.2.3. Eddy tracking and trajectory**

217 An eddy track consists of the trajectory of an eddy during its lifetime. The method  
218 proposed for eddy tracking [*Nencioli et al.*, 2010] is relatively simple and well-established.  
219 Once the eddy centers are detected, eddy tracks are identified by comparing the centers  
220 at successive time steps. The trajectory of a given eddy at the week  $n$  is updated by  
221 searching the next week  $n + 1$  the closest eddy of the same type (cyclone/anticyclone) in  
222 a restricted area around the position of the eddy at the week  $n$ . In the present study, the  
223 radius of the search area is  $45km$ , in other words the drifting speed of the eddy center  
224 cannot exceed  $6.5 km/day$  (i.e.  $7.5 cm.s^{-1}$ ). This value was chosen according to previous

225 studies [*Hamad et al.*, 2006; *Sutyryn et al.*, 2009] which shows that typical drifting speed  
226 of meso scale eddies in the eastern Mediterranean basin are around  $1 - 3 \text{ km/day}$ .

227 Vortices signature may also disappear (or be strongly smoothed) between consecutive  
228 maps, especially if their centers are located into the gaps between the satellites ground-  
229 tracks. To reduce these errors, we searched for the same eddy for two weeks after its  
230 disappearance and increased the search area up to  $67 \text{ km}$ . Nevertheless, we cannot guar-  
231 antee erroneous splitting of eddy tracks induced by measurements errors of the AVISO  
232 altimetric data set and the geostrophic velocity field derivation.

### 2.3. Comparison/validation of the optimized method with in-situ drifters and SST patterns

233 In order to estimate the accuracy of this optimized eddy detection algorithm we compare  
234 the trajectories, the size and the intensity of two vortices which were sampled during the  
235 EGYPT/EGITTO program [*Taupier-Letage*, 2007]. About 100 surface velocity drifters  
236 (SVP) drogued at 15m were released between fall 2005 to summer 2007 [*Gerin et al.*,  
237 2009]. A few of them, were launched in the core of the Ierapetra anticyclone and inside  
238 one Lybio-Egyptian eddy and they remained trapped several months inside their core.  
239 The drifter trajectories enable to reconstruct the tracks of the eddies and to quantify  
240 their surface velocities. Besides, several CTD transects were performed at the same time  
241 across these two anticyclones. A careful comparison of the eddies characteristics deduced  
242 from these in-situ measurements with the ones obtained from our optimized method is  
243 detailed below. Moreover, we checked on several SST fields the agreement of the detected  
244 eddies with the surface temperature patterns.

#### 2.3.1. Eddies trajectories

246 Among the hundred of SVP drifters launched during the EGYPT/EGITTO program,  
247 from 2005 to 2007, only a few of them get trapped inside eddies more than two months.  
248 Two surface drifters were trapped in the Ierapetra eddy generated in 2005 (IE05) and  
249 three other ones in the Lybio-Egyptian eddy (LE1). We use here the same notation as in  
250 *Gerin et al.* [2009] to label specific eddies. The kriging method [*Poulain and Zambianchi,*  
251 2007] was used to filter the dataset and extract the position  $(X_i, Y_i)$  and the instantaneous  
252 speed vector  $V_i$  of the drifters every six hours. When they are trapped, the drifters looped  
253 inside the eddy with a typical period of three to five days. Hence, when we filter out these  
254 rapid oscillations on both the latitude and the longitude dataset for these drifters, we can  
255 extract the slow evolution of the eddy center. The trajectory of the eddy center is then  
256 interpolated from all the trapped buoys for both anticyclones.

257 Among the five drifters launched in April 2006 inside the LE1 anticyclone, three drifters  
258 (b57312, b59774 and b59777) remained trapped in the eddy core for several months from  
259 April 2006 to September 2006. The westward drift of this anticyclone follows the Libyan  
260 shelf and keeps a constant distance ( $L = 55 - 65km$ ) between the vortex center and  
261 the 200m bathymetry [*Sutyris et al., 2009*], as shown in Fig.4. The trajectory deduced  
262 from the in-situ drifters during this period is in very good agreement with the eddy  
263 track obtained from the AVISO data set. Even if after six months the surface drifters  
264 escape from the eddy core, the automated eddy detection procedure we used allows us  
265 to follow the LE1 trajectory for twenty months. The date of the first detection of this  
266 vortex corresponds to early May 2006 when the algorithm identifies a new Lybio-Egyptian  
267 anticyclone detached from a pre-existing one. According to the AVISO velocity fields, this  
268 splitting event occurred along the Lybio-Egyptian coast in late April 2006. The further

269 evolution of the eddy is in agreement with the sea surface temperature field which showed  
270 that the LE1 anticyclone drifted westward along the Libyan shelf for more than one year  
271 [*Taupier-Letage*, 2008]. We confirm here that this eddy is long-lived and remains coherent  
272 for a quite long period: almost two years !

273 At the end of April 2006, four drifters were launched in the Ierapetra anticyclone IE05,  
274 two of them (b59748 and b59751) remained trapped inside the eddy core for almost three  
275 months until mid-July. At that time the IE05 merged with the young IE06, which appears  
276 at the end of June 2006 in the southeast corner of Crete. This merging, documented by  
277 *Taupier-Letage* [2008], is probably responsible of the ejection of the two surface drifters  
278 out of the core of IE05 in July 2006. During the three months period (April-July) the  
279 IE05 anticyclone slowly loops towards the North-East and the South-East Fig.5a). As  
280 for the previous case, a very good agreement is found between the trajectories deduced  
281 respectively from the in-situ drifters and our automated eddy track applied to the AVISO  
282 data set (Fig.5b ). Here again, the use of the geostrophic velocity fields deduced from  
283 the ADT enables us to follow the dynamical evolution of this coherent eddy along all its  
284 lifetime: from August 2005 to September 2007. These two intercomparisons show that our  
285 optimized method provides, for large meso-scale eddies, a correct localisation of the eddy  
286 center (i.e. the center of rotation) and therefore their trajectories at the grid accuracy  
287 ( $1/8^\circ$  for the AVISO velocity field).

### 288 **2.3.2. Eddies characteristics**

When they are trapped several weeks or months inside an eddy, the in-situ drifters  
may also provide quantitative estimations on the vortex size and its maximal velocity.  
Indeed, when the vortex center is accurately located we could calculate for each successive

position  $(X(t), Y(t))$  the radial distance  $R(t)$  from the drifter to the eddy center. Specific time intervals where the drifters trajectories remain almost circular were considered: the ellipticity  $\epsilon = 1 - b/a$  should be less than  $\epsilon_0 = 0.3$  where  $b$  and  $a$  are respectively the semi-minor and the semi-major axis. For all these circular loops  $i$  we calculate the time averaged radius  $R_i$  and the mean tangential velocity  $V_i$ . Fig.6 shows the data pair  $(R_i, V_i)$  measured for both the IE (left panel) and the LE (right panel) anticyclones. The intermittency of the local wind stresses or the small-scale wave activity induces dispersion in the drifter dynamics and a wide range of  $R_i$  values are explored while the drifters loop inside the eddy. Hence, assuming that the eddy profile remains almost the same during this three-four months period, with only a few drifters we can estimate the core velocity profiles of these two anticyclones. As a first guess we fit these tangential velocities with Gaussian velocity profiles (dashed lines) as a function of the radius  $r$  at each point of the eddy contour:

$$V(r) = V_{max} \frac{r}{R_{max}} \exp^{(1/2 - r^2/2R_{max}^2)} \quad (3)$$

According to these in-situ measurements the maximal tangential velocities  $V_{max} \simeq 35 \text{ cm.s}^{-1}$  of the Ierapetra anticyclone is reached when  $R_{max} \simeq 35 \text{ km}$  while for the Lybio-Egyptian eddy we get a larger velocity  $V_{max} \simeq 45 \text{ cm.s}^{-1}$  for a larger radius  $R_{max} \simeq 40 - 50 \text{ km}$ . These typical radii are much larger than the local deformation radius  $R_d = 8 - 12 \text{ km}$  in the area and the corresponding Burger number  $Bu = (R_d/R_{max})^2$  is therefore quite small  $Bu \simeq 0.04 - 0.08$ . Then, taking into account the local Coriolis parameter  $f$  at the eddy center latitude we can estimate the typical vortex Rossby

numbers

$$Ro = \frac{V_{max}}{fR_{max}} \quad (4)$$

Even if these two anticyclones have different size and intensity they have almost the same Rossby number  $Ro \simeq 0.12 - 0.13$ . These moderate values of  $Ro$  show that the centrifugal force is relatively small in comparison with the Coriolis force and that these circular eddies comply with the geostrophic balance assumptions. Moreover, we can also estimate the core vorticity  $\zeta(0)$  of these anticyclones according to the relation:

$$\zeta(r) = \partial_r V + \frac{V}{r} \quad (5)$$

For these Gaussian velocity profiles we get

$$\left| \frac{\zeta(0)}{f} \right| = 2 e^{1/2} Ro \simeq 0.4 - 0.43 \quad (6)$$

289 For such range of parameters ( $Ro \simeq 0.12$ ,  $\zeta(0) \simeq -0.4$ ,  $Bu \simeq 0.06$ ), these meso scale  
 290 anticyclones cannot be affected by unstable inertial perturbations [*Kloosterziel and van*  
 291 *Heijst*, 2006; *Carnevale et al.*, 2011; *Lazar et al.*, 2013a, b] and could therefore remain  
 292 stable and coherent for several months.

293 To compare these in-situ measurements to the ones obtained by the optimized algorithm  
 294 applied to the AVISO data-set, the temporal evolution of the typical radius  $R_{max}$  and the  
 295 maximum velocity  $V_{max}$  of the characteristic eddy contours for the IE05 (left panels) and  
 296 the LE1 (right panels) anticyclones are plotted in Fig.7 . Among the large dispersion of  
 297 data, we could observe a decay of the size and the intensity of the Ireapetra eddy from  
 298 the end of winter 2005 to the summer 2006. Then, the strong increase of the vortex  
 299 intensity from august to October 2006 appears to be correlated to the merging of the  
 300 old and weak IE05 with a new one formed and intensified by the Etesian winds during

301 this period. The merging event was clearly visible in July 2006 from consecutive SST  
302 images [Taupier-Letage, 2008]. On the other hand it is difficult to see in the Fig.7 any  
303 seasonal fluctuations for the LE anticyclone. The temporal variability of the  $R_{max}$  and the  
304  $V_{max}$  values is strong but there is no clear dynamical or meteorological reasons which could  
305 explain such variability which seems to be due to the intrinsic errors of the remote-sensing  
306 altimetry or the eddy detection algorithm. In order to make a relevant comparison between  
307 the automated detection algorithm and the surface drifters measurements we consider the  
308 temporal average of the vortex size and intensities during the weeks when surface drifters  
309 were trapped inside the eddies (grey areas in Fig.7). Moreover, two CTD transects were  
310 performed during the EGYPT-1 campaign (between April 19<sup>th</sup> to 21<sup>st</sup> 2006) across the  
311 diameter of both the IE05 and the LE1 anticyclones ([Taupier-Letage, 2007; Sutyrin et al.,  
312 2009]. Vertical sections of the geostrophic velocities were estimated from these CTD  
313 transects and we can then extract another independent estimation of  $R_{max}$  and  $V_{max}$  from  
314 in-situ measurements. The table 1 summarize this quantitative intercomparison. The  
315 characteristic eddy radius  $R_{max}$  of these large meso-scale eddies is correctly estimated by  
316 our optimized method. Nevertheless, we can notice that the geostrophic surface velocities,  
317 computed here from the 1/8° AVISO ADT, tend to underestimate the vortex intensity  
318 even if the vortex Rossby numbers are small. Similar underestimation of the intensity  
319 of large meso scale eddies, using the AVISO geostrophic velocities, was also observed for  
320 a wind-induced anticyclone in the wake of Madeira island [Caldeira et al., 2014]. It is  
321 expected that the coarse resolution AVISO data tend to smooth down the intensity of  
322 vortices having a radius ( $R_{max} = 30 - 40km$ ) too close to the AVISO grid ( $\Delta x \simeq 14km$   
323 for the present case). According to the recent analysis of Chelton et al. [2011], the SSH

324 fields of the AVISO Reference Series, have been filtered to attenuate Gaussian-like features  
325 with e-folding radii shorter than roughly  $40km$ .

326 These two examples show that satellite altimetry provides the most useful data set  
327 to follow, with an efficient eddy tracking algorithm, the trajectories of long-lived eddies  
328 at the ocean surface. If, the typical radius  $R_{max}$  of these two large meso-scale vortices  
329 are correctly estimated by the characteristic contours provided by the algorithm, their  
330 intensities  $V_{max}$  along this contour tend to be underestimated. Hence, the quantitative  
331 characterization of more intense (larger Rossby number) or smaller vortices ( $R_{max} \leq$   
332  $15 - 25km$ ) from coarse gridded satellite-based measurements will be much less accurate  
333 and should be considered with care.

### 334 **2.3.3. Comparison with SST patterns**

335 Unlike standard altimetry products, the sea surface temperature or the sea color data  
336 sets could exhibit the signatures of surface oceanic structures (currents, eddies and fila-  
337 ments) at high resolution. Indeed, when the wind stress is weak the surface temperature  
338 will be advected by the surface oceanic circulation as a passive tracer. Hence, the local  
339 temperature gradients may reveal the presence of coherent structures at both meso and  
340 submeso scale due to the  $1km$  resolution of the NOAA-AVHRR SST images. Fig.8 shows  
341 the SST image taken the 18<sup>th</sup> of June 2006. Among the large number of images we down-  
342 loaded from the Cyprius Oceanographic Center, we select this one because it exhibits a  
343 wide number of patterns with a high contrast. During that day and the preceding ones  
344 the wind forcing was weak and the cloud coverage negligible in the area under study.  
345 Hence, we were able to follow the temporal evolution of the SST patterns during four  
346 consecutives days (from the 16 to the 19 June) and identify qualitatively the location of

347 many cyclonic (open triangle) and anticyclonic (filled circle) circulations (Fig. 8a). We  
348 consider here only the centers where a significant rotation of the SST patterns was identi-  
349 fied during the four days. For comparison we superimposed, in Fig.8b the same SST map  
350 and the characteristic eddy contours detected by our method applied to the geostrophic  
351 velocities provided by AVISO for the week 15–21 june 2006. We plot here all the detected  
352 eddies even those with short lifetime or with contour of high ellipticity.

353 We should first mention that the various patterns visible on this SST map reveal a tur-  
354 bulent surface circulation governed by several coherent vortices in a wide range of scales.  
355 Among this turbulent field few large-scale anticyclones, labeled IE ( $25.5^{\circ}E, 34.25^{\circ}N$ ), PE  
356 ( $25.5^{\circ}E, 34.25^{\circ}N$ ), LE ( $22.5^{\circ}E, 33.75^{\circ}N$ ) and HTE ( $29^{\circ}E, 33.5^{\circ}N$ ) in the Fig.8b, are iden-  
357 tified both from the SST patterns and from the AVISO velocities. For these four long-lived  
358 eddies the area delimited by the characteristic contour are in correct agreement with the  
359 SST patterns even if their shape and the center locations may differ. On the other hand,  
360 the large scale cyclonic contour (detected during several weeks in the AVISO field) located  
361 at the west of the IE anticyclone Fig.8b overestimate the size of the cyclonic SST pattern  
362 located in the same area Fig.8a. We should mention that the SST patterns are mainly  
363 due to the Lagrangian advection of temperature gradients and therefore, there is no direct  
364 correlation with the closed contours shown in Fig.8b which correspond to instantaneous  
365 streamlines. Besides, we observe that anticyclonic (cyclonic) vortex could correpond to a  
366 cold (warm) core SST signature. These surprising observations confirm that the surface  
367 temperature is advected here as a passive tracer and is not correlated to the deeper ther-  
368 mocline structure of these geostrophic eddies. We should also note that smaller eddies,  
369 especially those along the Libyo-Egyptian coast, are not detected or correctly located by

370 the characteristic contours we computed. This is mainly due to the limited resolution  
 371 and the systematic measurements errors along the coast of altimetry data sets. These  
 372 latter do not enable to resolve accurately small meso scale vortices ( $R_{max} \leq 15 - 25km$ )  
 373 close to the coastlines or to detect submeso scale structures below the deformation radius  
 374  $R_d$ . This example, clearly shows the limits of any eddy detection algorithm applied to a  
 375 coarse gridded velocity field. Hence, the main limitation of our analysis comes from the  
 376  $1/8^\circ$  resolution of the AVISO data set. Nevertheless, these few intercomparisons (even if  
 377 they do not provide any statistical proofs) show that our optimized eddy detection algo-  
 378 rithm could provide relevant detection and tracking for sufficiently large and long-lived  
 379 meso-scale eddies.

### 3. Generations and dynamics of *long-lived eddies* from 1993 to 2012

380 We present in this section a statistical analysis of the eddies detected by the automated  
 381 procedure from 1993 to 2012. We consider, in what follows, coherent structures having  
 382 closed streamlines that were tracked for at least 8 weeks. This minimal life time guarantee  
 383 the coherence and the robustness of the detected structures. Among them we discarded  
 384 the vortices which are, on average, too small ( $R_{max} \leq 15$  km) or too ellongated ( $\epsilon \geq 0.3$ )  
 385 and we get a first list of 908 detected eddies for the 20 years period. Then, we perform a  
 386 regional analysis on 270 *long-lived eddies*, which live more than six months and are able  
 387 to trap and transport heat, salt and biogeochemical species over a long distance.

#### 3.1. Cyclone - anticyclone asymmetry

388 According to Fig.9 a large majority of the detected eddies having a lifetime that exceeds  
 389 8 weeks are cyclonic. Indeed, among these 908 eddies 62% are cyclonic and 38% are

390 anticyclonic. Nevertheless, this ratio is reversed if we only consider *long-lived eddies*.  
391 Indeed, when the lifetime exceeds six months the anticyclones become dominant. More  
392 than 80% of the eddies which were tracked for more than a year are anticyclonic. This  
393 dominance of anticyclones among the long lived eddies was observed throughout most of  
394 the Ocean [*Chelton et al.*, 2011]. However, this asymmetry appears to be more pronounced  
395 in eastern mediterranean basin. According to the statistical analysis of *Chelton et al.*  
396 [2011] the dominance of anticyclones in World Ocean occurs only when their lifetime  
397 exceeds 9 – 10 months, see Fig. 2 of *Chelton et al.* [2011].

398 Fig.10 analyses the size distribution as a function of the eddy lifetime. Large vortices  
399 ( $R_{max} > 32km$ ) which lived more than 21 weeks were predominantly anticyclonic while  
400 smaller eddies ( $R_{max} < 32km$ ) which lived shorter are mainly cyclonic (Fig.10). To  
401 explain the predominance of anticyclones among large-scale eddies, when the eddy radius  
402 becomes larger than the deformation radius, several studies were devoted to the specific  
403 stability of anticyclonic vortices in rotating shallow-water flows [*Arai and Yamagata*, 1994;  
404 *Stegner and Dritschel*, 2000; *Baey and Carton*, 2002]. Moreover, stable anticyclones tend  
405 to remain coherent within a turbulent flow [*Polvani et al.*, 1994; *Arai and Yamagata*, 1994;  
406 *Linden et al.*, 1995] and they were found to be more robust to external strain perturbations  
407 than cyclonic eddies [*Graves et al.*, 2006]. Idealized laboratory experiments [*Perret et al.*,  
408 2006a, b] and numerical simulations *Perret et al.* [2006a, b]; *Dong et al.* [2007], have  
409 shown that when the ratio of the vortex Rossby number  $Ro$  over the Burger number  $Bu =$   
410  $(R_d/R_{max})^2$  becomes large, anticyclones remain coherent and circular, whereas cyclones  
411 tend to be elongated and distorted. Besides, if we take into account the weak beta effect,  
412 which may affect large-scale oceanic eddies, several studies [*Matsuura and Yamagata*, 1982;

413 *Nycander and Sutyrin, 1992; Stegner and Zeitlin, 1995, 1996*] reveal that cyclonic eddies  
414 are strongly affected by the Rossby wave dispersion while anticyclones remain robust and  
415 coherent for a much longer time. Hence, both the vortex stability, the nonlinear vortex-  
416 vortex interactions and the Rossby wave dispersion lead to the predominance of large-scale  
417 anticyclones among the long-lived eddies of the eastern Mediterranean sea.

### 3.2. Generation areas of long-lived eddies

418 In order to detect the formation areas of long-lived eddies along the coasts we plot in  
419 Fig.11 the first detection points of the eddies which were tracked more than six months  
420 during the 20 years of analysis. Once they are formed, vortices could travel a long distance,  
421 up to several hundreds of kilometers (see Fig.4), over the whole basin. If the full trajectory  
422 of all these 96 long-lived eddies were plotted, all the Eastern Mediterranean Basin would be  
423 filled by the eddy tracks. But if we plot only the initial formation points, the distribution  
424 is not uniform and specific areas could be identified. For instance, Fig.11a shows a higher  
425 density of these first detection points in the well-known areas of the Ierapetra (IE) or the  
426 Pelops (PE) eddies. The formations of large meso-scale anticyclones in these two areas  
427 were already observed and discussed in previous studies [*Hamad et al., 2005; Gerin et al.,*  
428 *2009; Amitai et al., 2010; Menna et al., 2012*]. It confirms that the first detection point  
429 computed by our tracking algorithm can identify the generation area of long-lived eddies.

430 Note that such type of analysis differs from the previous ones [*Isern-Fontanet et al.,*  
431 *2006; Amitai et al., 2010; Menna et al., 2012*] which focused on areas of intense Eddy  
432 Kinetic Energy (EKE). Indeed, the kinetic energy fluctuations could be induced by the  
433 variabilities of strong currents, a large number of intense vortices having a short lifetime  
434 or by the drift of long-lived vortices which were formed elsewhere. On the other hand,

435 the region where long-lived eddies are formed and detached regularly from the coast will  
436 necessarily be a region of strong EKE. Hence, the following analysis which focuses on the  
437 first detection points (i.e. possible generation areas) of long-lived structures will be more  
438 selective and will contain only a fraction of the intense EKE areas.

439 The figure Fig.11 clearly shows the predominance of anticyclonic vortices (59 anticy-  
440 clones and 41 cyclones) and that a large majority of these meso-scale eddies tend to appear  
441 in the northern part of the basin (above  $33.5^{\circ}N$ ). Only a few long-lived anticyclones are  
442 first detected in the southern part along the Lybio-Egyptian coast. If the orographic wind  
443 forcing or the instabilities of surface current are standard mechanisms for the generation  
444 of coherent vortices we should mention that a vortex splitting that may occur in the (tur-  
445 bulent) open sea will lead to the formation (i.e. first detection) of a new vortex. Indeed,  
446 we observed on the high resolution SST field few episodes of such vortex splitting in the  
447 middle of the basin. Hence, to refine the analysis and identify possible mechanisms of  
448 eddy formation, we study in the next sub-section how the detection/formation points of  
449 these long-lived eddies are related to the seasonal variability.

### 3.3. Seasonal variability, possible formation mechanisms and eddies trajectories

450 We plot in figures Fig.12 and Fig.13 the first detection points of anticyclones and cy-  
451 clones, during the 20 years of analysis, for the four seasons. We take into account the  
452 coherent eddies which were tracked more than two months (open circles) and the long-  
453 lived eddies that survive more than six months (filled circles). As in Fig.11, we can see in  
454 some specific areas a higher density of points. We focus in what follows on these areas,

455 delimited by dashed contours, which may correspond to formation regions for coherent  
456 and *long-lived* eddies.

#### 457 *Ierapetra Eddies* (IE)

458 The intense anticyclonic eddy located southeast of Crete, i.e. the Ierapetra eddy, is one  
459 of the most extensively studied vortex in this area. Several works [*Larnicol et al.*, 1995;  
460 *Hamad et al.*, 2006; *Amitai et al.*, 2010; *Menna et al.*, 2012] have observed or quantified  
461 its annual variability. The anticyclone is generated in summer, becomes fully developed in  
462 late summer or early fall and often disappears in the following spring. The Fig.12 confirms  
463 that the first detection of the IE eddies occurs mainly during the summer period (June  
464 21<sup>st</sup> - September 20<sup>th</sup>). Nevertheless, in few cases, 3 among the 20 years, the formation of  
465 the Ierapetra anticyclone was not detected. Several times, it survived the whole year and  
466 merged with a new anticyclone at the summer period leading to a longer lifetime for our  
467 detection algorithm. Such case is visible, for instance, in Fig.7c where the intensity of the  
468 IE anticyclone decayed from December to June 2006 and increased again in July 2006.  
469 The detection stops in July 2007, almost two years after the first detection in August 2005.  
470 A careful analysis of the eddy tracking shows that a merging event occurs, mid-July 2006,  
471 between the IE05 anticyclone and the IE06 which emerges and grows in the southeast  
472 tip of Crete in early July 2006. These various scenarios and dynamical evolutions may  
473 explain the past discussions and controversy on the permanent or the recurrent nature of  
474 this large and intense anticyclone.

475 The high density of first detection point during the summer period is in agreement  
476 with the *Horton et al.* [1994] hypothesis that the Ierapetra eddy is mainly forced by the  
477 Etesian winds. In order to quantify the seasonal variability of the wind forcing in the

478 sub-basin under study, we used the ALADIN data set [Tramblay *et al.*, 2013] and we  
479 compute the monthly winds climate over the 1993 – 2012 period. Each of these months  
480 corresponds to the arithmetic mean of the twenty monthly average wind data. We plot  
481 in Fig.14a the wind stress vectors and the wind stress curl amplitude for the mean June  
482 which is the month having the highest wind-stress curl induced in the south of Crete by  
483 the Etesian winds. The strong wind-shears found in this area are in agreement with the  
484 previous analysis of Bakun and Agostini [2001] and Amitai *et al.* [2010]. Moreover, we  
485 select a circular domain (IE\_area in Fig.14a) centered at  $(26.75^{\circ}E, 34.75^{\circ}N)$  with a  $45km$   
486 radius where a large number of IE eddies were initially detected. The Fig.14c shows that  
487 the mean wind stress curl in this IE\_area start to increases in spring an reaches its highest  
488 values in June and July. The persistence of an anticyclonic wind-shear (i.e. negative  
489 wind-stress curl) is expected to induce a local Ekman downwelling and therefore favor the  
490 formation of anticyclones. Therefore, the spatial and temporal correlation between the  
491 maximum of south-east Etesian winds which occurs in late spring and early summer (Fig.  
492 14) and the first detection of the Ierapetra eddies in summer (Fig. 12) confirms that the  
493 anticyclonic wind-shear is a major forcing. The role of local wind-stress as a driver for  
494 oceanic eddies was also studied in the lee of oceanic mountainous islands such as Hawai  
495 [Calil *et al.*, 2008; Jia *et al.*, 2011] or Madeira [Couvelard *et al.*, 2012; Caldeira *et al.*,  
496 2014].

497 The typical radius of the detected IE is on average ( $R_{max} \simeq 35 - 40km$ ) much larger  
498 than the local deformation radius. They are the most intense eddies in the basin with a  
499 mean Rossby number  $Ro \simeq 0.15$ . We plot in Fig.15 few characteristic trajectories of these  
500 IE anticyclones. Once the eddy is formed it may escape from the coast and stays relatively

501 close to it with an irregular motion or travel towards the south. The slow southwestward  
502 drift is the most frequent trajectory (about 60%) but in a few cases we also observed a  
503 slow eastward drift.

#### 504 *Pelops Eddies* (PE)

505 As for the Ierapetra eddy, there is a general agreement that the Pelops anticyclone (PE),  
506 located southwest of the Peloponnese [*Matteoda and Glenn, 1996*], is mainly triggered by  
507 the wind-stress curl [*Ayoub et al., 1998*]. Some authors [*Marullo et al., 1999*] also con-  
508 sider the meandering of the Atlantic Ionian stream (AIS) as a complementary mechanism  
509 for the generation of the PE anticyclone. Our analysis exhibits, in Autumn (Fig.12),  
510 a strong density of first detection points located in an area of significant anticyclonic  
511 wind-stress curl (PE\_area in Fig.14). In the late summer, the Etesian winds turns from  
512 south-east (Fig.14a) to south (Fig.14b). This new direction amplifies the wind accelera-  
513 tion and therefore the wind-shear in the Peloponnese-Cretan strait. The monthly winds  
514 evolution in this specific area (PE\_area delimited by dashed circle in Fig.14b) shows that  
515 the maximum wind-stress curl is reached in September. The previous analysis of *Bakun*  
516 *and Agostini* [2001], also shows that the maximum intensity of the Ekman downwelling,  
517 located in the same area, occurs in Autumn, mainly in October or November according to  
518 their Fig.4f. Therefore, the fact that the Pelops anticyclone tend to be detected later than  
519 the Ierapetra eddy, is well correlated to the increases of the local wind-shear in the respec-  
520 tive formation areas. This spatio-temporal correlation gives a new evidence that the wind  
521 is one of the major mechanism which drives the generation of the Pelops anticyclones.

522 As for the IE eddy, we observe from the eddy tracking algorithm that the PE anticyclone  
523 may survive more than a year and merge with another anticyclone formed in the same

524 area. Hence, many authors mention a permanent eddy [*Robinson et al.*, 1991; *Theocharis*  
525 *et al.*, 1993; *Matteoda and Glenn*, 1996] or large scale gyre subject to seasonal variability  
526 [*Larnicol et al.*, 2002].

### 527 *Herodotus Trough Eddies* (HTE)

528 Another area with a high concentration of first detection points is located along the  
529 Herodotus Trough (Fig.11). Surprisingly, all these points stand along the 3000m isobath of  
530 this mediterranean trough. A large number of meso scale anticyclones, often called Mersa  
531 Matruh Eddies, were observed in this area [*Horton et al.*, 1994; *Ayoub et al.*, 1998; *Larnicol*  
532 *et al.*, 1995; *Hamad et al.*, 2006; *Amitai et al.*, 2010; *Menna et al.*, 2012]. Following the  
533 classification proposed by *Gerin et al.* [2009] we called the eddies the Herodotus Trough  
534 Eddies (HTE) to emphasize the fact that they were initially detected along the Herodotus  
535 Trough. Several mechanisms of formation were proposed in previous studies. *Brenner*  
536 [1989] detected and surveyed a long-lived warm core eddy which appears to have formed  
537 off the coast of Egypt as a meander of the Libyo Egyptian Current (LEC). Hence, he  
538 first suggested that the coastal current instability could be the main source of HTE.  
539 According to other studies [*Robinson et al.*, 1991; *Malanotte-Rizzoli and Bergamasco*,  
540 1991; *Theocharis et al.*, 1993] the “Mersa-Matruh Gyre” is a permanent feature. It was  
541 also described as a system of several eddies [*Horton et al.*, 1994; *Ayoub et al.*, 1998] or  
542 due to the meander of the MMJ [*Larnicol et al.*, 2002].

543 According to our analysis of 20 years of AVISO velocity fields, the HTE seems to be  
544 mainly formed in spring and summer. We have checked that, even if the wind stress could  
545 be strong, the wind-stress curl is always negligible in this area (Fig.14). Hence, the HTE  
546 eddies cannot be wind-induced and we should look for other formation mechanism. The

547 typical trajectories of the anticyclones which were formed close to the Egyptian coast  
548 are plotted in Fig.16. All these anticyclones emerged from a coastal meander and once  
549 they escape from the coast they propagate northeastward and transport coastal waters  
550 towards the basin center, as the warm core eddy observed by *Brenner* [1989]. Hence,  
551 the instabilities of the LEC or the local changes of the mean shelf slope could explain the  
552 formation of large meanders or meso-scale eddies in this area. Some laboratory experiment  
553 have shown that when a buoyant coastal current flow from a steep to a gentle slope, the  
554 widening of the isobaths may serve as an accumulation point for the meanders generated on  
555 the steep slope [*Wolfe and Cenedese*, 2006]. On average, the typical size and vortex Rossby  
556 number of the detected HTE were about  $R_{max} = 40 - 45km$  and  $Ro \simeq 0.1$ . Nevertheless,  
557 several merging or splitting events were also observed leading to a complex eddy dynamics  
558 and a significant variability of the eddy radius. Most of the HTE anticyclones formed (i.e.  
559 first detection point) above  $33^{\circ}N$  result from the splitting of a pre existing anticyclone.  
560 A splitting event occurred in the HTE area in June 2005, according to the analyses of  
561 successive SST images. This intercomparison confirms that vortex splitting occurs (it is  
562 not an eddy detection artefact) and could be one of the recurrent mechanisms, for the  
563 formation of coherent structures in the area. Hence, the Herodotus Trough bathymetry  
564 seems to impact both the detachment point of large meanders of the LEC and the splitting  
565 of the meso scale HTE which travel northeastward off the Egyptian coast.

#### 566 *Benghazi Eddies (BE)*

567 Along the Libyan coast, one area centered at  $20^{\circ}E, 32.5^{\circ}N$  along the Benghazi shelf  
568 focused our attention. We noticed in this area (hereafter referred to as BE) several fo-  
569 mation points of long-lived anticyclones (Fig.12). We noticed from a thorough analysis of

570 the geostrophic surface circulation (AVISO ADT data set) that meanders of a transient  
 571 alongshore current often form in that area. The first detection points identified in the BE  
 572 area correspond to the detachment of finite amplitude meanders generating meso-scale  
 573 anticyclones. On average, the typical size and vortex Rossby number of the detected BE  
 574 were about  $R_{max} \simeq 30 - 35km$  and  $Ro \simeq 0.07$ . The size, the intensity and also the  
 575 mean life time ( $\tau \simeq 35$  weeks) of the anticyclonic BE are slightly smaller than the other  
 576 large-scale anticyclones formed in the basin, especially the IE, the PE and the HTE. Their  
 577 smaller size and their reduced lifetime may explain why these eddies were not discussed  
 578 or identified in previous studies. The analysis of the characteristic BE trajectories shows  
 579 that some eddies may stay at the same location for several months (Fig.17b and Fig.17d).  
 580 These specific events seem to indicate that the shelf bathymetry of the BE area could  
 581 favor the formation or the accumulation of anticyclonic vortices. Moreover, as for the  
 582 Herodotus Trough area, there is no significant and recurrent wind stress curl along the  
 583 Libyo-Egyptian coast that may trigger the formation of large scale vortices. Hence, the  
 584 formation of *long-lived* anticyclones in the BE area may find a plausible explanation in  
 585 some instability process or the impact of the coastal bathymetry on the surface circulation.

586 According to Fig.17c), when a Benghazi eddy is formed slightly away from the shelf  
 587 slope, , this long-lived eddy propagates in the middle of the basin with an average westward  
 588 drift speed of  $V_d \simeq 0.4 - 0.45km/day$ . In order to estimate the maximum phase speed  $V_\beta$  of  
 589 Rossby waves associated to the first baroclinic mode we should take into account the local  
 590 deformation radius  $R_d = 10 - 12km$ . The standard Rossby wave phase speed is about  $V_\beta =$   
 591  $\beta R_d^2 \simeq 0.15 - 0.2 km/day$  where  $\beta$  is the beta parameter at the eddy latitude  $\theta \simeq 33^\circ N$ .  
 592 If we consider the westward drift of an isolated anticyclone in a reduced-gravity shallow-

593 water model [*Nycander and Sutyrin, 1992; Stegner and Zeitlin, 1995, 1996*], nonlinear  
 594 effects induced by the finite isopycnal deviation may lead to a supercritical drift speed of  
 595  $V_d = V_\beta [1 + a(Bu/Ro)]$ , where  $a$  is a geometrical factor that depends on the eddy shape.  
 596 If we take  $a \simeq 1$  in the first approximation, we get  $V_d \simeq 0.35 - 0.45 km/day$  when the  
 597 vortex Rossby number  $Ro \simeq 0.07$  and  $(R_d/R_{max}) = \sqrt{Bu} \simeq 0.3$ . Hence, in that case  
 598 the westward drift speed of the BE anticyclone is in good agreement with the theoretical  
 599 speed of a *long-lived* and coherent anticyclone driven only by the beta effect.

### 600 *Western Cretan Eddies (WCE)*

601 The Western Cretan Gyre, a cyclonic circulation located at the southwest of Crete, was  
 602 identified in previous studies according to its SST signature and few in-situ data [*Matteoda*  
 603 *and Glenn, 1996*]. It was often described as a permanent gyre in regional circulation  
 604 scheme [*Robinson et al., 1991; Theocharis et al., 1993*]. The Fig.8 exhibits a cold SST  
 605 signal in that area without any clear eddy pattern while a cyclonic eddy was detected  
 606 by our analysis of the AVISO data set (the dashed contour centered at  $(23^\circ E, 34.7^\circ N)$  in  
 607 Fig.8). The SST signature of these cold core eddies could be masked or perturbed by local  
 608 warming of the sea surface layer during the summer months and it may explain the lack of  
 609 detection from the SST maps. Nevertheless, according to the Fig.13 a high concentration  
 610 of first detection points, labeled WCE, are detected during the summer period. The  
 611 location of the WCE area coincides with the location of strong cyclonic wind-stress curl  
 612 induced by the Etesian winds in June and July (Fig.14). Similar upwelling, induced by  
 613 the south-east Etesian winds in the late summer, was also detected in the same this area  
 614 by *Bakun and Agostini [2001]*. The average size and vortex Rossby number of these  
 615 cyclonic eddies are about  $R_{max} \simeq 25 km$  and  $Ro \simeq 0.07$ , which is significantly smaller and

616 less intense than the anticyclonic IE. Hence, the acceleration of the Etesian winds and  
617 the strong wind-shear induced by the Cretan orography tends to generate cyclonic (the  
618 WCE's) and anticyclonic (the IE's) eddies in the near wake of this elongated island. As it  
619 is expected for large island, when the island diameter is larger than the local deformation  
620 radius [*Perret et al.*, 2006b, 2010], the anticyclonic eddies are larger and more intense  
621 than the cyclonic ones for the same wake forcing.

#### 4. Summary and conclusions

622 This study provides a new statistical analysis of long-lived eddies, which stay coherent  
623 more than six months, in the Eastern Mediterranean Sea. Unlike many other studies  
624 which tend to quantify the long-term mean circulation or the areas of intense eddy kinetic  
625 energy (EKE), we focused on the few specific areas where *long-lived* eddies are gener-  
626 ated recurrently and we try to estimate their size, their intensity and their characteristic  
627 trajectories from the surface geostrophic velocity fields provided by AVISO.

628 We first optimized the *Nencioli et al.* [2010] eddy tracking algorithm and implement a  
629 new procedure based on the computation of the Local and Normalized Angular Momentum  
630 (*LNAM*) to identify the eddy centers. This new procedure appears to be more robust  
631 and more efficient than the initial one for the analysis of coarse gridded velocity fields  
632 such as the  $1/8^\circ$  AVISO data set. Moreover, we checked our method on two meso-scale  
633 anticyclones, the LE and the IE vortices which were sampled with several in-situ drifters  
634 and CTD transects during the EGYPT campaign in 2006. We verified that our new  
635 algorithm provides a correct estimation of the eddy center and its characteristic radius  
636  $R_{max}$  corresponding to the maximal tangential velocity  $V_{max}$ .

637 The analysis of 20 year of AVISO surface velocities, from 1993 to 2012, reveals a strong  
638 cyclone-anticyclone asymmetry of meso scale vortices. The dominance of anticyclones  
639 among the *long-lived* eddies was observed through the statistical eddy lifetime histogram  
640 of the global ocean [Chelton *et al.*, 2011] but, this study shows that this asymmetry is  
641 much more pronounced in eastern Mediterranean basin. We found that large vortices  
642 which lived more than six months were predominantly anticyclonic with a characteristic  
643 radius  $R_{max}$  exceeding by a factor two or three the local deformation radius  $R_d$  while  
644 smaller eddies lived shorter and are mainly cyclonic. The predominance of recurrent or  
645 semi-permanent anticyclones in the Mediterranean sea is often mentioned in previous  
646 studies according to various in-situ observations. But, among the surface drifters which  
647 where launched and trapped several months inside eddy cores most of them were deployed  
648 inside large scale anticyclones. This bias in the drifters deployment may have led to an  
649 overdetection of anticyclones. On the other hand, studies based on altimetric data set  
650 [Isern-Fontanet *et al.*, 2006] show a much larger number of cyclones and only a slight  
651 predominance of anticyclonic structures in the global circulation maps. Our study is the  
652 first one which quantifies precisely this asymmetry as a function of the eddy size and their  
653 lifetime. This significant predominance of long-lived and large-scale anticyclones could be  
654 explained by theoretical studies on the stability [Arai and Yamagata, 1994; Stegner and  
655 Dritschel, 2000; Baey and Carton, 2002] and the robustness of large-scale anticyclones  
656 on the beta-plane [Nycander and Sutyrin, 1992; Stegner and Zeitlin, 1995, 1996] or in a  
657 turbulent eddy field [Polvani *et al.*, 1994; Arai and Yamagata, 1994; Linden *et al.*, 1995].  
658 Nevertheless, this asymmetry could also be induced by the specific mechanisms of eddy  
659 generation in this area.

660 In order to estimate the formation areas of *long-lived* vortices, we provide the seasonal  
661 maps of the first detection points for both cyclones and anticyclones cumulated over  
662 the 20 years of analysis. The regions with higher density of points are considered as  
663 preferential formation areas. The spatial and temporal correlations of these specific areas  
664 with the seasonal wind-stress curl or the bottom bathymetry provides some evidences and  
665 suggest hypothesis on the various dynamical mechanisms which may govern the recurrent  
666 formation of meso scale eddies in the eastern basin. This study confirms that the formation  
667 of both the Ierapetra and the Pelops eddies are strongly correlated to the local Ekman  
668 downwelling induced the acceleration/channeling of the Etesian winds on both side of the  
669 Cretan orography. Besides, we provide some evidence that the smaller cyclonic eddies  
670 formed at the southwest of Crete (Western Cretan Eddies) may also be induced by the  
671 same wind forcing. On the other hand, the meso-scale anticyclones formed along the  
672 Libyan or the Egyptian coasts are not directly correlated to the wind variability. We  
673 noticed that the 3000m isobath of the Herodotus Trough seems to have a strong impact  
674 on the formation of large scale anticyclones along and off the Mersa Matruh coast. Besides,  
675 several eddies formed close to the coast follows this isobath and few of them split in the  
676 central basin. Hence, the strong variation of the shelf slope in this area tends to control  
677 the transport of coastal water to the open sea. Moreover, we indentify a new formation  
678 area, not discussed before, along the curved shelf of the Benghazi coast. The intensity and  
679 also the mean life time of these anticyclonic Benghazi Eddies (BE) are slightly smaller  
680 ( $R_{max} \simeq 30 - 35km$ ) than the other meso-scale anticyclones ( $R_{max} \simeq 35 - 40km$ ) formed  
681 in the basin. If we hypothesis that these anticyclones result from the instability of a  
682 coastal current along the shelf, the steepness of the topographic slope in that area will

683 tend to reduce the wavelength of the unstable perturbations [*Pennel et al.*, 2012; *Poulin*  
 684 *et al.*, 2013] and therefore the size of coastal eddies generated from the coastal meanders.  
 685 Nevertheless, in the next future, a more detailed analysis of the bathymetric impact on  
 686 the coastal circulation should be done in that area to identify the possible formation  
 687 mechanism.

688 **Acknowledgments.** This work was funded by the ANR-Astrid Project SYNBIOS  
 689 (ANR 11 ASTR 014 01). Besides, Nadia Mkhinini thanks the national supports from  
 690 DGA (Délégation Générale de l'Armement) and EDX (École Doctorale Polytechnique)  
 691 in the context of the ADETOC project. We thanks Florence Sevault and Samuel  
 692 Somot from CNRM/Mto-France for the atmospheric daily winds of ALADIN used  
 693 in this study. Satellites data are Ssalto/Duacs Sea level anomalies and geostrophic  
 694 velocity anomalies on a  $1/8^\circ$  regular grid over the Mediterranean Sea taken from  
 695 the AVISO website : [http://www.aviso.altimetry.fr/en/data/products/sea-surface-height-](http://www.aviso.altimetry.fr/en/data/products/sea-surface-height-products/regional.html)  
 696 [products/regional.html](http://www.aviso.altimetry.fr/en/data/products/sea-surface-height-products/regional.html). Sea surface temperature map are taken from the Cyprus Oceanographic  
 697 Center <http://www.oceanography.ucy.ac.cy/cycofos/index.html>. The eddy detec-  
 698 tion algorithm is available by contact to the authors.

## Appendix A: Comparison with the standard Okubo-Weiss method

699 The Okubo-Weiss parameter  $W = \sigma_n^2 + \sigma_s^2 - \zeta^2$  evaluates the relative amplitude between  
 700 the local deformation and the local rotation where  $\sigma_n = \frac{\partial u}{\partial x} - \frac{\partial v}{\partial y}$ ,  $\sigma_s = \frac{\partial v}{\partial x} + \frac{\partial u}{\partial y}$  and  
 701  $\zeta = \frac{\partial v}{\partial x} - \frac{\partial u}{\partial y}$  are the shearing deformation rate, the straining deformation rate and the  
 702 vertical component of vorticity, respectively. The vortex interior is dominated by vorticity  
 703 and thus, negative values of  $W$  are expected in the vortex core. The pioneering work of

704 Isern-Fontanet (2003, 2004, 2006) suggests to use the specific contours corresponding to  
705 the threshold  $W_0 = -0.2\sigma_w$  to identify the vortex cores, where  $\sigma_w$  is the standard deviation  
706 of the  $W$  distribution among the domain. Another study (Chaigneau et al. 2008) suggests  
707 that the best compromise is a  $W_0$  value in the range  $-0.3\sigma_w \leq W_0 \leq -0.2\sigma_w$ .

708 Fig.18 shows the eddy detection using the OW method on the same surface velocity field  
709 used in Fig.3. The grayscale colorbar represents the intensity of the dimensionless  $W/f^2$   
710 parameter and the black solid line the standard threshold  $W_0 = -0.2\sigma_w$ . The Ierapetra  
711 ( $26.5^\circ$  E -  $34.3^\circ$  N) and the Pelops ( $21.8^\circ$  E -  $35.6^\circ$  N) eddies, are clearly identified on the  
712 Fig.18. However, in comparison with Fig.3, the OW method induces a strong excess of  
713 eddy detection. The curvature of the flow field, due to current meanders for instance, may  
714 induces a strong and localized vorticity which do not correspond to any coherent vortex  
715 with closed streamlines as detected by our optimized algorithm (Fig.3). Hence, the OW  
716 method induces a strong excess of detection.

## References

- 717 Amitai, Y., Y. Lehahn, A. Lazar, and E. Heifetz (2010), Surface circulation of the eastern  
718 Mediterranean Levantine basin: Insights from analyzing 14 years of satellite altimetry  
719 data, *Journal of Geophysical Research*, *115*(C10), C10,058+, doi:10.1029/2010jc006147.
- 720 Arai, M., and T. Yamagata (1994), Asymmetric evolution of eddies in rotating shallow  
721 water, *Chaos: An Interdisciplinary Journal of Nonlinear Science*, *4*(2), 163–175, doi:  
722 10.1063/1.166001.
- 723 Ayoub, N., P.-Y. Le Traon, and P. De Mey (1998), A description of the Mediterranean  
724 surface variable circulation from combined ERS-1 and TOPEX/POSEIDON altimetric

- 725 data, *Journal of Marine Systems*, 18(1-3), 3–40, doi:10.1016/s0924-7963(98)80004-3.
- 726 Baey, J. M., and X. Carton (2002), Vortex multipoles in two-layer rotating shallow-water  
727 flows, *Journal of Fluid Mechanics*, 460, 151–175, doi:10.1017/s0022112002008170.
- 728 Bakun, A., and V. N. Agostini (2001), Seasonal patterns of wind-induced up-  
729 welling/downwelling in the Mediterranean Sea, *Scientia Marina*, 65(3), 243–257.
- 730 Brenner, S. (1989), Structure and evolution of warm core eddies in the eastern  
731 Mediterranean Levantine Basin, *J. Geophys. Res.*, 94(C9), 12,593–12,602, doi:  
732 10.1029/jc094ic09p12593.
- 733 Caldeira, R. M. A., A. Stegner, X. Couvelard, I. B. Araújo, P. Testor, and A. Lorenzo  
734 (2014), Evolution of an oceanic anticyclone in the lee of Madeira Island: In situ and  
735 remote sensing survey, *Journal of Geophysical Research: Oceans*, 119(2), 1195–1216,  
736 doi:10.1002/2013jc009493.
- 737 Calil, P. H. R., K. J. Richards, Y. Jia, and R. R. Bidigare (2008), Eddy activity in the lee  
738 of the Hawaiian Islands, *Deep Sea Research Part II: Topical Studies in Oceanography*,  
739 55(10-13), 1179–1194, doi:10.1016/j.dsr2.2008.01.008.
- 740 Carnevale, G. F., R. C. Kloosterziel, P. Orlandi, and D. D. J. A. van SOMMEREN (2011),  
741 Predicting the aftermath of vortex breakup in rotating flow, *Journal of Fluid Mechanics*,  
742 669, 90–119, doi:10.1017/s0022112010004945.
- 743 Chaigneau, A., A. Gizolme, and C. Grados (2008), Mesoscale eddies off Peru in altime-  
744 ter records: Identification algorithms and eddy spatio-temporal patterns, *Progress in*  
745 *Oceanography*, 79(2-4), 106–119, doi:10.1016/j.pocean.2008.10.013.
- 746 Chaigneau, A., G. Eldin, and B. Dewitte (2009), Eddy activity in the four major upwelling  
747 systems from satellite altimetry (1992-2007), *Progress in Oceanography*, 83(1-4), 117–

- 748 123, doi:10.1016/j.pocean.2009.07.012.
- 749 Chelton, D. B., M. G. Schlax, R. M. Samelson, and R. A. de Szoeke (2007), Global  
750 observations of large oceanic eddies, *Geophysical Research Letters*, *34*(15), L15,606+,  
751 doi:10.1029/2007gl030812.
- 752 Chelton, D. B., M. G. Schlax, and R. M. Samelson (2011), Global observations  
753 of nonlinear mesoscale eddies, *Progress in Oceanography*, *91*(2), 167–216, doi:  
754 10.1016/j.pocean.2011.01.002.
- 755 Couvelard, X., R. M. A. Caldeira, I. B. Araújo, and R. Tomé (2012), Wind me-  
756 diated vorticity-generation and eddy-confinement, leeward of the Madeira Island:  
757 2008 numerical case study, *Dynamics of Atmospheres and Oceans*, *58*, 128–149, doi:  
758 10.1016/j.dynatmoce.2012.09.005.
- 759 Dong, C., J. C. McWilliams, and A. F. Shchepetkin (2007), Island Wakes in Deep Water,  
760 *J. Phys. Oceanogr.*, *37*(4), 962–981, doi:10.1175/jpo3047.1.
- 761 Gerin, R., P. M. Poulain, I. Taupier-Letage, C. Millot, S. B. Ismail, and C. Sammari  
762 (2009), Surface circulation in the Eastern Mediterranean using drifters (2005-2007),  
763 *Ocean Science Discussions*, *6*(1), 525–555, doi:10.5194/osd-6-525-2009.
- 764 Graves, L. P., J. C. McWilliams, and M. T. Montgomery (2006), Vortex evolution due to  
765 straining: a mechanism for dominance of strong, interior anticyclones, *Geophysical &  
766 Astrophysical Fluid Dynamics*, *100*(3), 151–183, doi:10.1080/03091920600792041.
- 767 Hamad, N., C. Millot, and I. Taupier-Letage (2005), A new hypothesis about the surface  
768 circulation in the eastern basin of the mediterranean sea, *Progress in Oceanography*,  
769 *66*(2-4), 287–298, doi:10.1016/j.pocean.2005.04.002.

- 770 Hamad, N., C. Millot, and I. Taupier-Letage (2006), The surface circulation in the eastern  
771 basin of the Mediterranean Sea, *SCIENTIA MARINA*, *70*(3), 457–503.
- 772 Horton, C., J. Kerling, G. Athey, J. Schmitz, and M. Clifford (1994), Airborne expend-  
773 able bathythermograph surveys of the eastern Mediterranean, *Journal of Geophysical*  
774 *Research*, *99*(C5), 9891+, doi:10.1029/94jc00058.
- 775 Isern-Fontanet, J., E. García-Ladona, and J. Font (2003), Identification of Marine Eddies  
776 from Altimetric Maps, *J. Atmos. Oceanic Technol.*, *20*(5), 772–778, doi:10.1175/1520-  
777 0426(2003)20%3C772:iomefa%3E2.0.co;2.
- 778 Isern-Fontanet, J., J. Font, E. García-Ladona, M. Emelianov, C. Millot, and I. Taupier-  
779 Letage (2004), Spatial structure of anticyclonic eddies in the Algerian basin (Mediterranean Sea) analyzed using the Okubo-Weiss parameter, *Deep Sea Research Part II: Topical Studies in Oceanography*, *51*(25-26), 3009–3028, doi:10.1016/j.dsr2.2004.09.013.
- 780 Isern-Fontanet, J., E. García-Ladona, and J. Font (2006), Vortices of the Mediterranean Sea: An Altimetric Perspective, *J. Phys. Oceanogr.*, *36*(1), 87–103, doi:  
781 10.1175/jpo2826.1.
- 782 Isern-Fontanet, J., B. Chapron, G. Lapeyre, and P. Klein (2006b), Potential use of microwave sea surface temperatures for the estimation of ocean currents, *Geophysical Research Letters*, *33*(24), doi:10.1029/2006gl027801.
- 783 Jia, Y., P. H. R. Calil, E. P. Chassignet, E. J. Metzger, J. T. Potemra, K. J. Richards, and  
784 A. J. Wallcraft (2011), Generation of mesoscale eddies in the lee of the Hawaiian Islands, *Journal of Geophysical Research*, *116*(C11), C11,009+, doi:10.1029/2011jc007305.
- 785 Kloosterziel, R. C., and G. J. F. van Heijst (2006), An experimental study of unstable  
786 barotropic vortices in a rotating fluid, *Journal of Fluid Mechanics*, *223*, 1–24, doi:

793 10.1017/s0022112091001301.

794 Larnicol, G., P.-Y. Le Traon, N. Ayoub, and P. De Mey (1995), Mean sea level and surface  
795 circulation variability of the Mediterranean Sea from 2 years of TOPEX/POSEIDON  
796 altimetry, *Journal of Geophysical Research*, *100*(C12), 25,163+, doi:10.1029/95jc01961.

797 Larnicol, G., N. Ayoub, and P. Y. Le Traon (2002), Major changes in Mediterranean  
798 Sea level variability from 7 years of TOPEX/Poseidon and ERS-1/2 data, *Journal of*  
799 *Marine Systems*, *33-34*, 63–89, doi:10.1016/s0924-7963(02)00053-2.

800 Lazar, A., A. Stegner, and E. Heifetz (2013a), Inertial instability of intense stratified  
801 anticyclones. Part 1. Generalized stability criterion, *Journal of Fluid Mechanics*, *732*,  
802 457–484, doi:10.1017/jfm.2013.412.

803 Lazar, A., A. Stegner, R. Caldeira, C. Dong, H. Didelle, and S. Viboud (2013b), Inertial  
804 instability of intense stratified anticyclones. Part 2. Laboratory experiments, *Journal of*  
805 *Fluid Mechanics*, *732*, 485–509, doi:10.1017/jfm.2013.413.

806 Linden, P. F., B. M. Boubnov, and S. B. Dalziel (1995), Source&#8211;sink turbu-  
807 lence in a rotating stratified fluid, *Journal of Fluid Mechanics*, *298*, 81–112, doi:  
808 10.1017/s0022112095003235.

809 Malanotte-Rizzoli, P., and A. Bergamasco (1991), The wind and thermally driven cir-  
810 culation of the eastern Mediterranean Sea. Part II: the Baroclinic case, *Dynamics of*  
811 *Atmospheres and Oceans*, *15*(3-5), 355–419, doi:10.1016/0377-0265(91)90026-c.

812 Marullo, S., R. Santoleri, P. Malanotte-Rizzoli, and A. Bergamasco (1999), The sea sur-  
813 face temperature field in the Eastern Mediterranean from advanced very high reso-  
814 lution radiometer (AVHRR) data, *Journal of Marine Systems*, *20*(1-4), 63–81, doi:  
815 10.1016/s0924-7963(98)00071-2.

- 816 Matsuura, T., and T. Yamagata (1982), On the Evolution of Nonlinear Planetary Ed-  
817 dies Larger than the Radius of Deformation, *J. Phys. Oceanogr.*, *12*(5), 440–456, doi:  
818 10.1175/1520-0485(1982)012%3C0440:oteonp%3E2.0.co;2.
- 819 Matteoda, A. M., and S. M. Glenn (1996), Observations of recurrent mesoscale eddies  
820 in the eastern Mediterranean, *Journal of Geophysical Research*, *101*(C9), 20,687+, doi:  
821 10.1029/96jc01111.
- 822 Menna, M., P.-M. Poulain, G. Zodiatis, and I. Gertman (2012), On the surface circu-  
823 lation of the Levantine sub-basin derived from Lagrangian drifters and satellite al-  
824 timetry data, *Deep Sea Research Part I: Oceanographic Research Papers*, *65*, 46–58,  
825 doi:10.1016/j.dsr.2012.02.008.
- 826 Millot, C., and R. Gerin (2010), The Mid-Mediterranean Jet Artefact, *Geophys. Res.*  
827 *Lett.*, *37*(12), L12,602+, doi:10.1029/2010gl043359.
- 828 Millot, C., and I. Taupier-Letage (2005), Circulation in the Mediterranean Sea, in *The*  
829 *Mediterranean Sea, Handbook of Environmental Chemistry*, vol. 5K, edited by A. Saliot,  
830 pp. 29–66, Springer Berlin Heidelberg, doi:10.1007/b107143.
- 831 Morrow, R., F. Birol, D. Griffin, and J. Sudre (2004), Divergent pathways of cy-  
832 clonic and anti-cyclonic ocean eddies, *Geophys. Res. Lett.*, *31*(24), L24,311+, doi:  
833 10.1029/2004gl020974.
- 834 Nencioli, F., C. Dong, T. Dickey, L. Washburn, and J. C. McWilliams (2010), A  
835 Vector Geometry-Based Eddy Detection Algorithm and Its Application to a High-  
836 Resolution Numerical Model Product and High-Frequency Radar Surface Velocities  
837 in the Southern California Bight, *J. Atmos. Oceanic Technol.*, *27*(3), 564–579, doi:  
838 10.1175/2009jtecho725.1.

- 839 Nycander, J., and G. G. Sutyrin (1992), Steadily translating anticyclones on the  
840 beta plane, *Dynamics of Atmospheres and Oceans*, 16(6), 473–498, doi:10.1016/0377-  
841 0265(92)90002-b.
- 842 Pennel, R., A. Stegner, and K. Béranger (2012), Shelf impact on buoyant coastal current  
843 instabilities., *Journal of Physical Oceanography*, 42(1).
- 844 Perret, G., A. Stegner, M. Farge, and T. Pichon (2006a), Cyclone-anticyclone asymmetry  
845 of large-scale wakes in the laboratory, *Physics of Fluids (1994-present)*, 18(3), 036,603+,  
846 doi:10.1063/1.2179387.
- 847 Perret, G., A. Stegner, T. Dubos, J. M. Chomaz, and M. Farge (2006b), Stability of  
848 parallel wake flows in quasigeostrophic and frontal regimes, *Physics of Fluids (1994-  
849 present)*, 18(12), 126,602+, doi:10.1063/1.2397563.
- 850 Perret, G., T. Dubos, and A. Stegner (2010), How Large-Scale and Cyclogeostrophic  
851 Barotropic Instabilities Favor the Formation of Anticyclonic Vortices in the Ocean, *J.  
852 Phys. Oceanogr.*, 41(2), 303–328, doi:10.1175/2010jpo4362.1.
- 853 Pinardi, N., I. Allen, E. Demirov, P. De Mey, G. Korres, A. Lascaratos, P.-Y. Le Traon,  
854 C. Maillard, G. Manzella, C. Tziavos, et al. (2003), The mediterranean ocean forecasting  
855 system: first phase of implementation (1998-2001), in *Annales Geophysicae*, vol. 21, pp.  
856 3–20.
- 857 Polvani, L. M. M., J. C. C. McWilliams, M. A. A. Spall, and R. Ford (1994), The coherent  
858 structures of shallow-water turbulence: Deformation-radius effects, cyclone/anticyclone  
859 asymmetry and gravity-wave generation., *Chaos (Woodbury, N.Y.)*, 4(2), 177–186.
- 860 Poulain, P.-M., and E. Zambianchi (2007), Surface circulation in the central Mediter-  
861 ranean Sea as deduced from Lagrangian drifters in the 1990s, *Continental Shelf Re-*

- 862 *search*, 27(7), 981–1001, doi:10.1016/j.csr.2007.01.005.
- 863 Poulain, P.-M., M. Menna, and E. Mauri (2012), Surface Geostrophic Circulation of  
864 the Mediterranean Sea Derived from Drifter and Satellite Altimeter Data, *J. Phys.*  
865 *Oceanogr.*, 42(6), 973–990, doi:10.1175/jpo-d-11-0159.1.
- 866 Poulin, F., A. Stegner, M. Hernández-Arencibia, A. Marrero-Díaz, and P. Sangrà (2013),  
867 Steep shelf stabilisation of the bransfield coastal current: linear stability analysis, *Jour-*  
868 *nal of Physical Oceanography*, (2013).
- 869 Rio, M. H., P. M. Poulain, A. Pascual, E. Mauri, G. Larnicol, and R. Santoleri (2007), A  
870 Mean Dynamic Topography of the Mediterranean Sea computed from altimetric data,  
871 in-situ measurements and a general circulation model, *Journal of Marine Systems*, 65(1-  
872 4), 484–508, doi:10.1016/j.jmarsys.2005.02.006.
- 873 Robinson, A. R., M. Golnaraghi, W. G. Leslie, A. Artegiani, A. Hecht, E. Lazzoni,  
874 A. Michelato, E. Sansone, A. Theocharis, and U. Ünlüata (1991), The eastern Mediter-  
875 ranean general circulation: features, structure and variability, *Dynamics of Atmospheres*  
876 *and Oceans*, 15(3-5), 215–240, doi:10.1016/0377-0265(91)90021-7.
- 877 Sadarjoen, I. A., F. H. Post, B. Ma, D. C. Banks, and H. G. Pagendarm (1998), Selective  
878 visualization of vortices in hydrodynamic flows, in *Visualization & #039;98. Proceedings*,  
879 pp. 419–422, IEEE, doi:10.1109/visual.1998.745333.
- 880 Sangrà, P., A. Pascual, A. Rodríguez-Santana, F. Machín, E. Mason, J. C. McWilliams,  
881 J. L. Pelegrí, C. Dong, A. Rubio, J. Arístegui, A. Marrero-Díaz, A. Hernández-Guerra,  
882 A. Martínez-Marrero, and M. Auladell (2009), The Canary Eddy Corridor: A major  
883 pathway for long-lived eddies in the subtropical North Atlantic, *Deep Sea Research Part*  
884 *I: Oceanographic Research Papers*, 56(12), 2100–2114, doi:10.1016/j.dsr.2009.08.008.

- 885 Schonten, M. W., W. P. M. de Ruijter, P. J. van Leeuwen, and J. R. E. Lutjeharms (2000),  
886 Translation, decay and splitting of Agulhas rings in the southeastern Atlantic Ocean,  
887 *Journal of Geophysical Research*, *105*(C9), 21,913+, doi:10.1029/1999jc000046.
- 888 Sorgente, R., A. Olita, P. Oddo, L. Fazioli, and A. Ribotti (2011), Numerical simulation  
889 and decomposition of kinetic energy in the central mediterranean: insight on mesoscale  
890 circulation and energy conversion., *Ocean Science*, *7*(4).
- 891 Souza, J. M. A. C., de Boyer Montégut, and P. Y. Le Traon (2011), Comparison between  
892 three implementations of automatic identification algorithms for the quantification and  
893 characterization of mesoscale eddies in the South Atlantic Ocean, *Ocean Science*, *7*(3),  
894 317–334, doi:10.5194/os-7-317-2011.
- 895 Stegner, A., and D. G. Dritschel (2000), A numerical investigation of the stability of iso-  
896 lated shallow water vortices, *JOURNAL OF PHYSICAL OCEANOGRAPHY*, *30*(10),  
897 2562–2573, times Cited: 15.
- 898 Stegner, A., and V. Zeitlin (1995), What can asymptotic expansions tell us about  
899 large-scale quasi-geostrophic anticyclonic vortices?, *Nonlinear Processes in Geophysics*,  
900 *2*(3/4), 186–193.
- 901 Stegner, A., and V. Zeitlin (1996), Asymptotic expansions and monopolar solitary Rossby  
902 vortices in barotropic and two-layer models, *Geophysical & Astrophysical Fluid Dynam-*  
903 *ics*, *83*(3-4), 159–194, doi:10.1080/03091929608208965.
- 904 Sutyrin, G., A. Stegner, I. Taupier-Letage, and S. Teinturier (2009), Amplification of a  
905 Surface-Intensified Eddy Drift along a Steep Shelf in the Eastern Mediterranean Sea,  
906 *J. Phys. Oceanogr.*, *39*(7), 1729–1741, doi:10.1175/2009jpo4106.1.

- 907 Taupier-Letage, I. (2007), the egypt/egitto teams: New elements on the surface circulation  
908 in the eastern basin of the mediterranean, rapp, *Comm. Int. Mer. Medit.*
- 909 Taupier-Letage, I. (2008), On the Use of Thermal Images for Circulation Studies: Appli-  
910 cations to the Eastern Mediterranean Basin, in *Remote Sensing of the European Seas*,  
911 edited by V. Barale and M. Gade, pp. 153–164, Springer Netherlands, doi:10.1007/978-  
912 1-4020-6772-3\_12.
- 913 Teinturier, S., A. Stegner, H. Didelle, and S. Viboud (2010), Small-scale instabilities of  
914 an island wake flow in a rotating shallow-water layer, *Dynamics of Atmospheres and*  
915 *Oceans*, *49*(1), 1–24, doi:10.1016/j.dynatmoce.2008.10.006.
- 916 Theocharis, A., D. Georgopoulos, A. Lascaratos, and K. Nittis (1993), Water masses  
917 and circulation in the central region of the Eastern Mediterranean: Eastern Ionian,  
918 South Aegean and Northwest Levantine, 1986-1987, *Deep Sea Research Part II: Topical*  
919 *Studies in Oceanography*, *40*(6), 1121–1142, doi:10.1016/0967-0645(93)90064-t.
- 920 Tramblay, Y., D. Ruelland, S. Somot, R. Bouaicha, and E. Servat (2013), High-resolution  
921 med-cordex regional climate model simulations for hydrological impact studies: a first  
922 evaluation in morocco, *Hydrology and Earth System Sciences Discussions*, *10*(5), 5687–  
923 5737.
- 924 Wolfe, C. L., and C. Cenedese (2006), Laboratory experiments on eddy generation by a  
925 buoyant coastal current flowing over variable bathymetry, *Journal of physical oceanog-*  
926 *raphy*, *36*(3), 395–411.

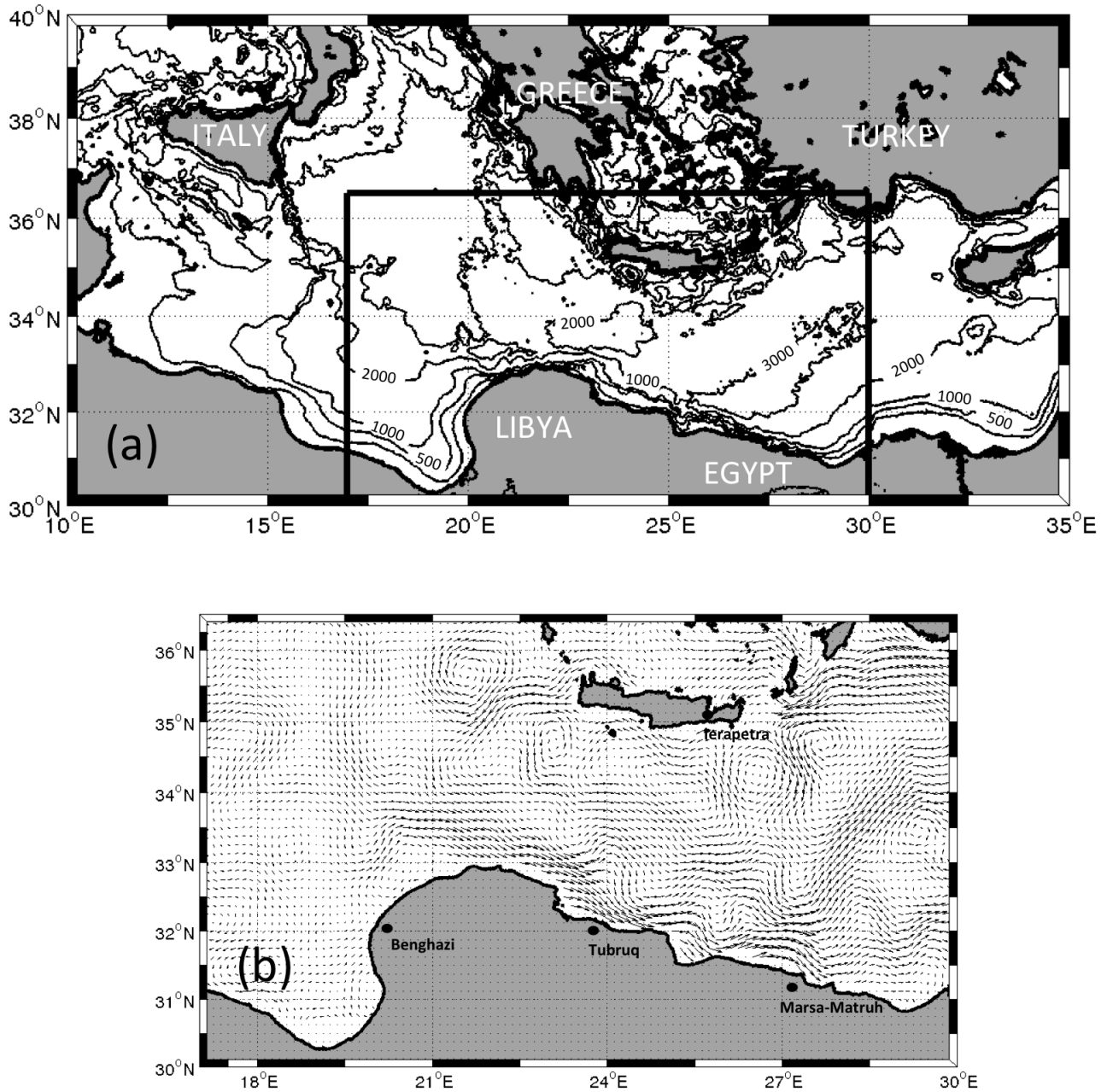


**Figure 1.** Bathymetry of the Eastern Mediterranean Sea (a) and the twenty years average (1993-2012) of the surface geostrophic velocities computed from AVISO ADT products (b), in the sub-basin area [17°E - 30°E, 30°N - 36°N].

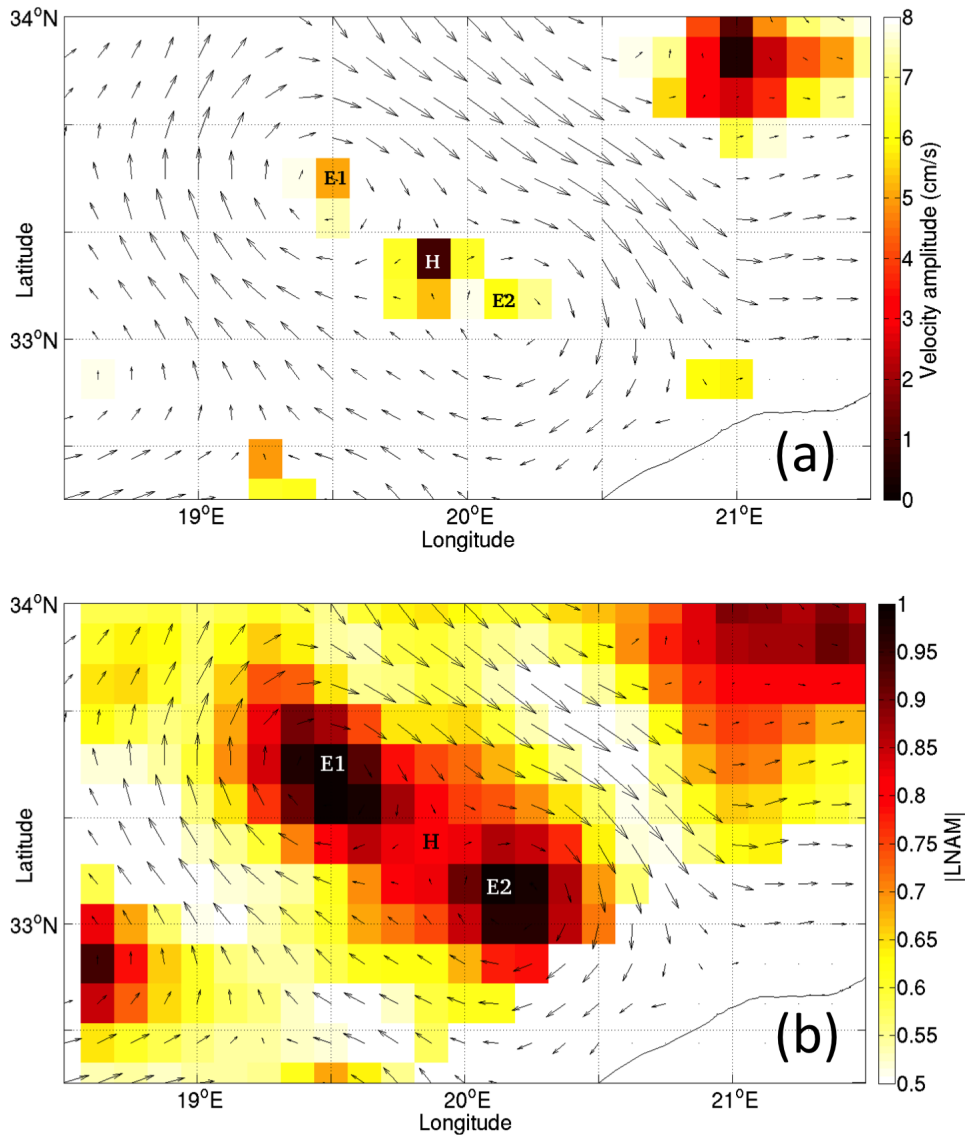


**Figure 2.** Example of surface geostrophic velocity fields, provided by AVSIO, with two close vortices. The upper panel (a) shows the three grid points ( $H$ ,  $E_1$  and  $E_2$ ) corresponding to local velocity minima. In this case the lowest velocity value is found in the hyperbolic point  $H$  and not in the points  $E_1$  or  $E_2$  which are close to the eddy centers (elliptical points). The magnitude of the  $LNAM$  parameter is shown, for the same velocity field, in the lower panel (b). In this case, the two elliptical centers ( $E_1$  and  $E_2$ ) coincides with the highest values of  $|LNAM|$ .

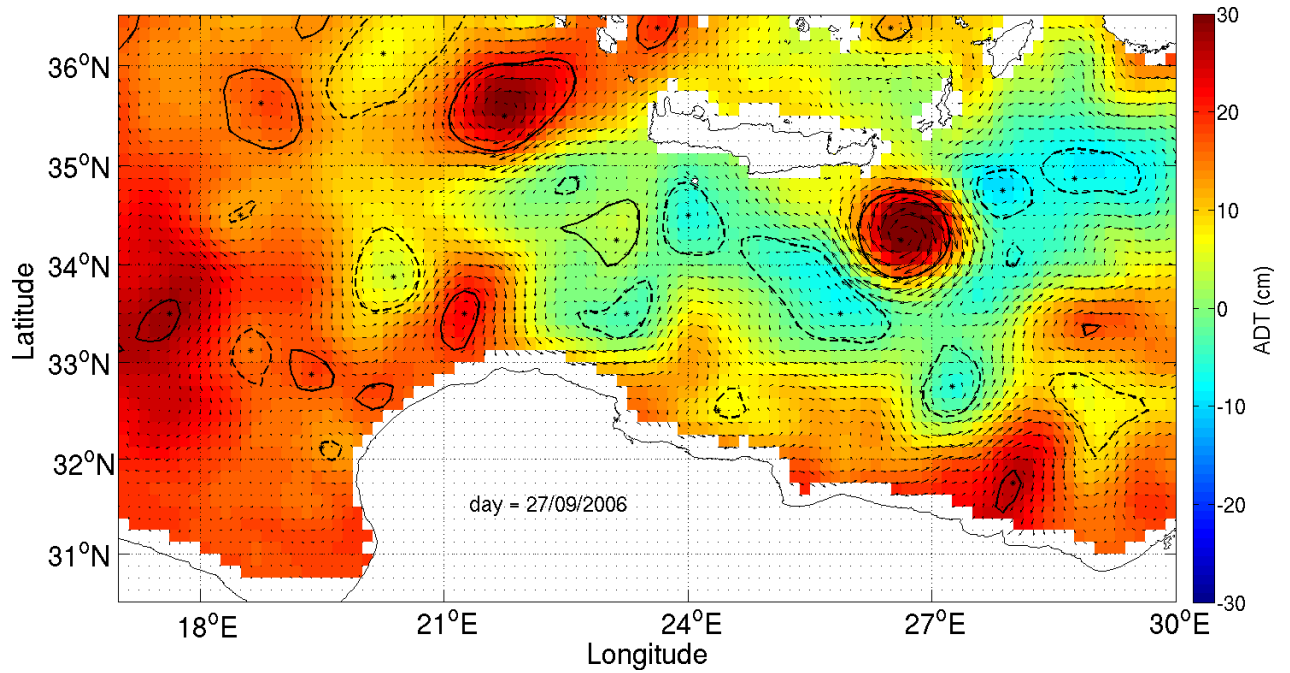


**Figure 3.** Eddies detected by the optimized algorithm on the AVISO geostrophic velocity field (September 27<sup>th</sup> 2006) derived from the ADT altimetry data set. The black stars corresponds to the eddy centers identified with the *LNAM* parameter while the solid lines (dashed lines) corresponds to the anticyclonic (cyclonic) vortex contours.

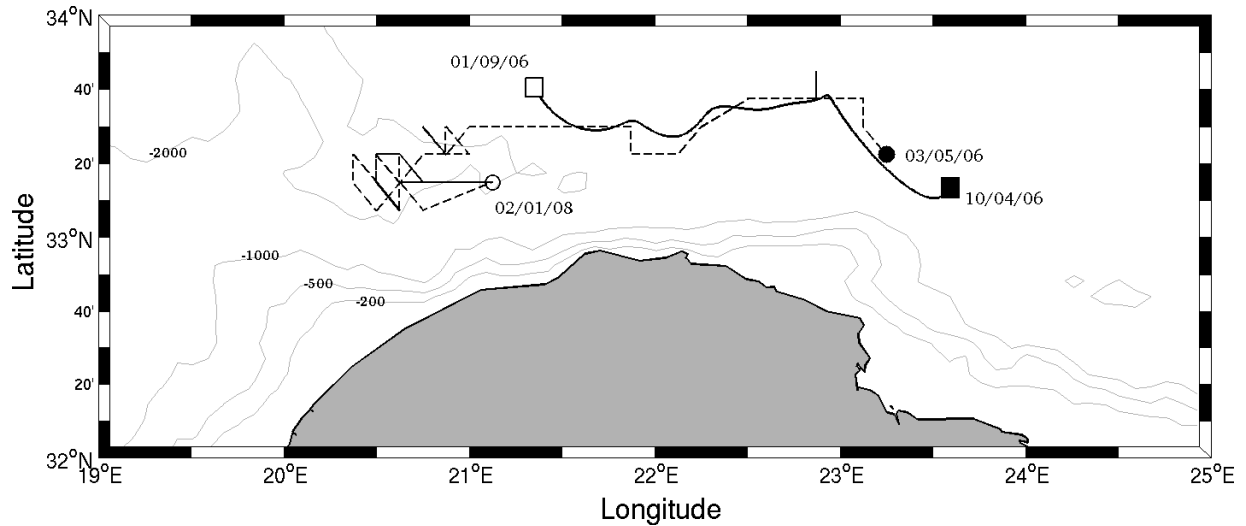


**Figure 4.** Trajectories of the Libyo-Egyptian eddy LE1, from April 2006 to January 2008, according to the analysis of surface drifter dataset (solid line) and according to the eddy tracking algorithm applied to the AVISO dataset (dashed line). The initial (final) position of the detected eddy center is plotted with a filled (open) mark. The -200 m, -500m, -1000m and -3000m isobaths of the shelf bathymetry are drawn (grey lines).

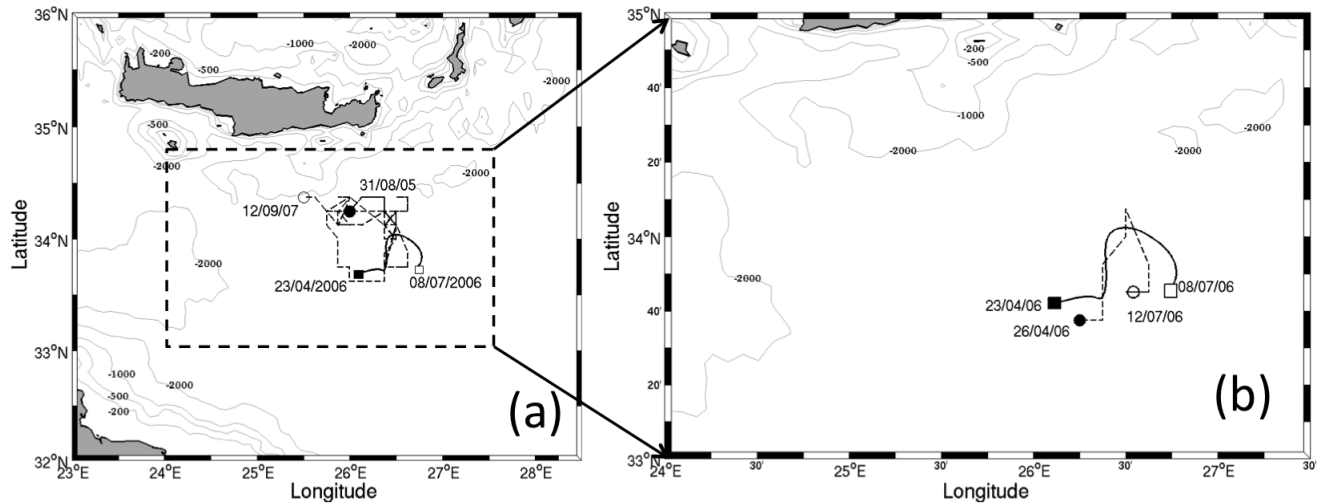


**Figure 5.** Trajectories of the Ierapetra eddy according to the analysis of surface drifter dataset (solid line) and according to the eddy tracking algorithm applied to the AVISO dataset (dashed line). The initial (final) position of the detected eddy center is plotted with a filled (open) mark. The right panel (b) compares the two trajectories only during the three months period (April-July 2006) when surface drifters get trapped inside the eddy core.

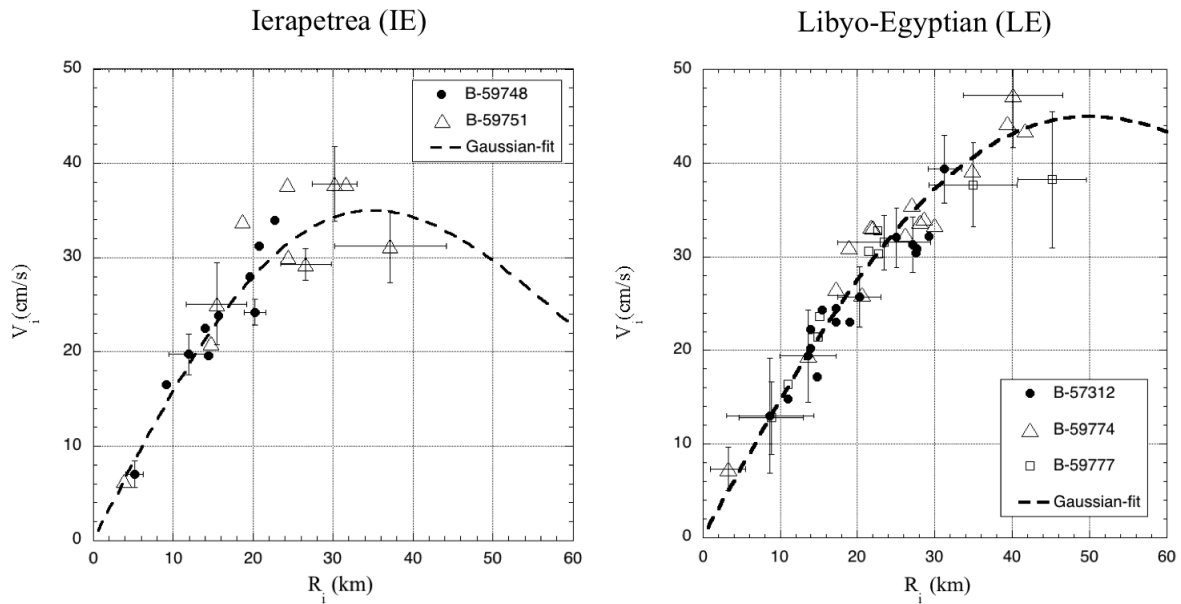


**Figure 6.** Mean tangential velocities  $V_i$  of the surface drifters, trapped in the IE eddy (left panel) or the LE eddy (right panel), plotted as a function of the average radius  $R_i$  for several circular loops  $i$ . The dashed line corresponds to a Gaussian profile fit according to the equation (3). The numbers  $B - 59748$ ,  $B - 59751$  corresponds to the drifters ID.

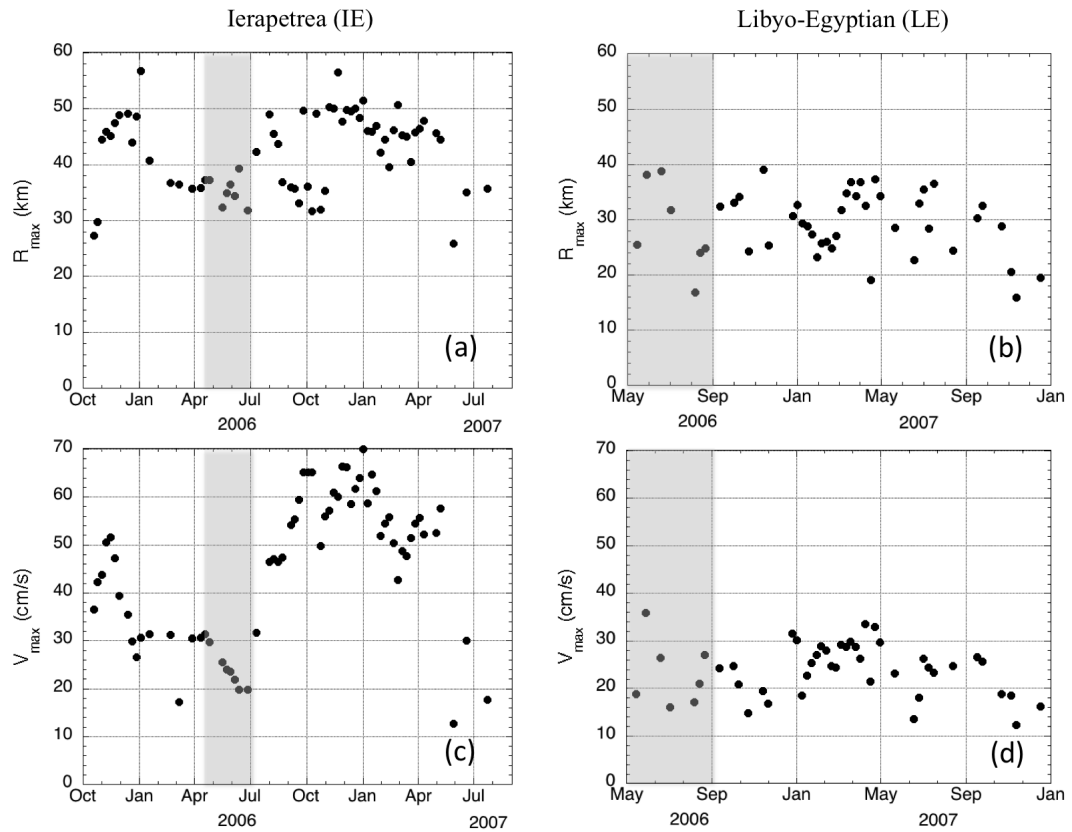


**Figure 7.** Temporal evolution of the radius  $R_{max}$  and the tangential velocity  $V_{max}$  of the Ierapetra eddies (a, c) and the Libyo-Egyptian eddy (b, d) according to the characteristic eddy contours given by the optimized algorithm. The grey areas represent the time period when the surface drifters were trapped inside each anticyclone.

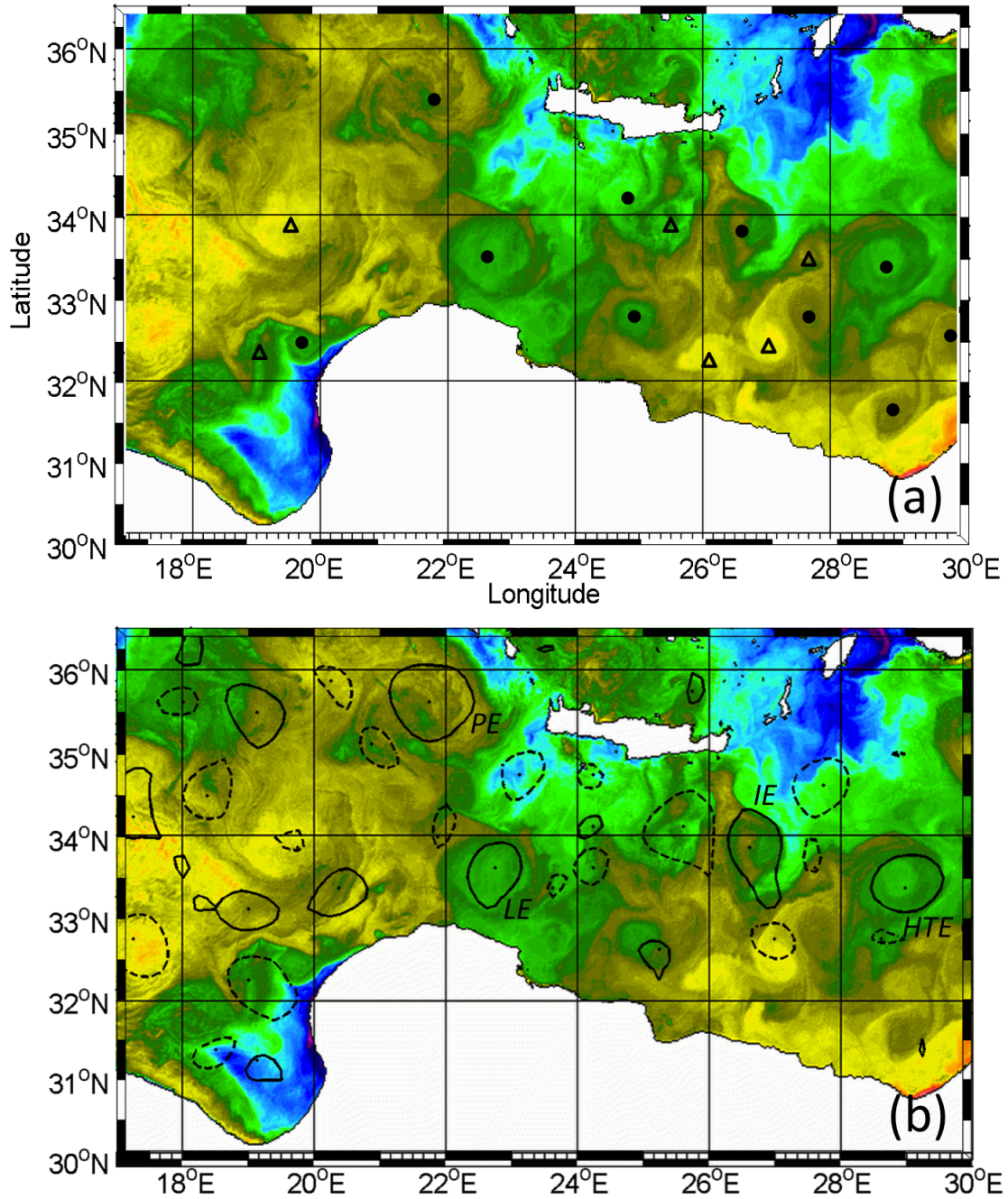


**Figure 8.** The upper panel (a) shows the centers of anticyclonic (filled circle) and cyclonic (triangle) motion identified on the SST field of the June 18<sup>th</sup> 2006 provided by the Cyprus Oceanographic Center. The lower panel (b) superimposed on the same SST field the contours of the anticyclonic (solid lines) and cyclonic (dashed lines) eddies detected by the optimized algorithm applied to the AVISO geostrophic velocity field (week 15 – 21, June 21<sup>st</sup> 2006).

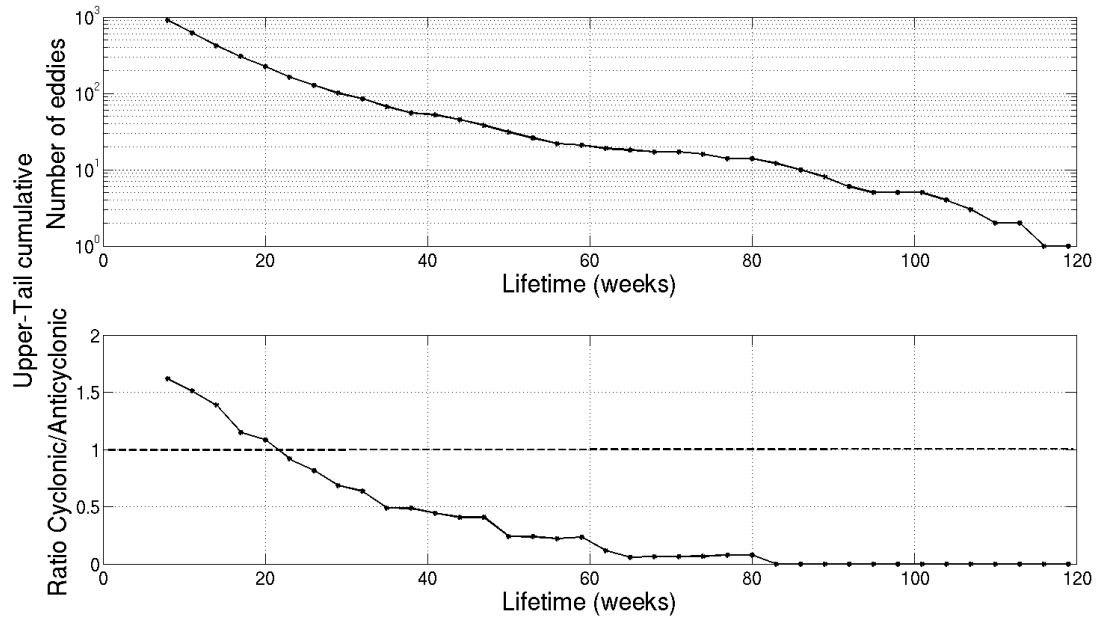


**Figure 9.** The upper-tail cumulative histograms (the number of eddies with lifetimes greater than or equal to each particular value along the abscissa) is plotted in the upper panel. The upper-tail cumulative histograms of the ratio cyclones/anticyclones is plotted in the lower panel. Note: for instance eddies with lifetimes  $\geq 8$  weeks ( $\geq 35$  weeks) the ratio cyclones/anticyclones is 1.6 (0.5).

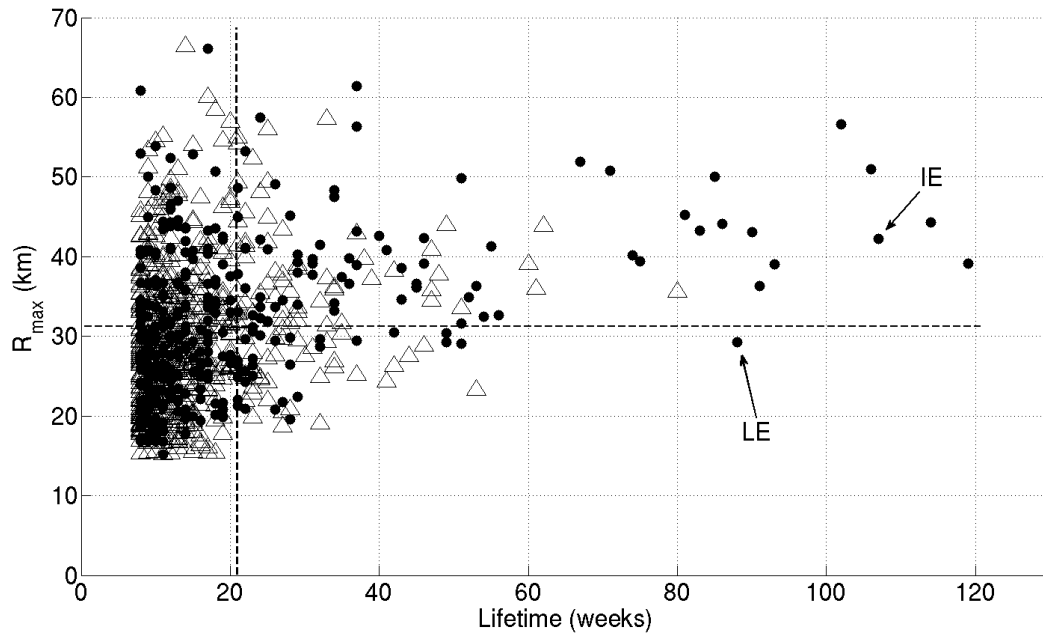


**Figure 10.** Mean eddy radius as a function of the eddy lifetime. The  $R_{max}$  value is here an averaged value over the whole lifetime of the eddies. Filled circle are used to represent the anticyclones while the open triangles represent the cyclones. The horizontal (vertical) dashed line corresponds to the threshold radius  $R_{max} = 32km$  (threshold lifetime  $\tau = 21$  weeks) where the ratio of cyclonic over anticyclonic eddies is equal to unity.

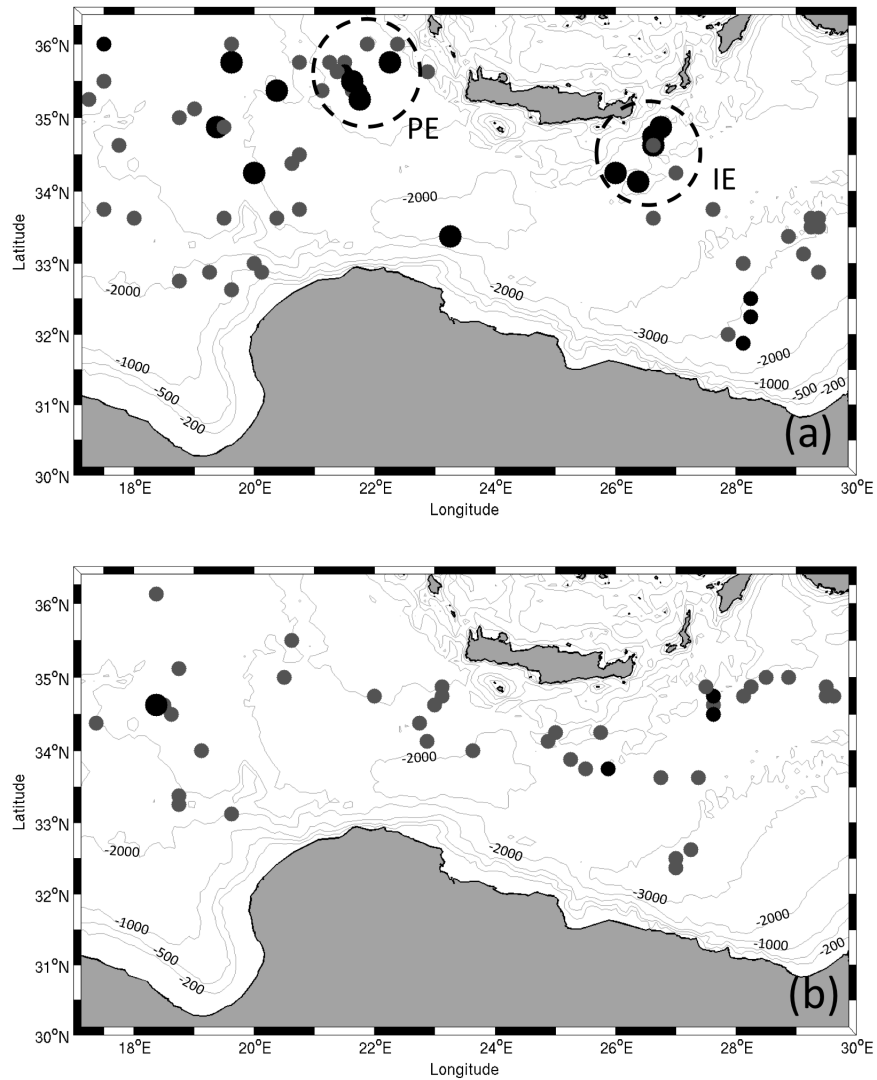


**Figure 11.** First detection points of long-lived anticyclones (a) and cyclones (b) during the 1993-2012 period. The dot sizes and colors correspond to the eddy lifetime :  $\tau_L = 6 - 12$  months (small grey circle),  $\tau_L = 12 - 18$  months (small black circle), more than 18 months (big black dots). The grey lines represent the  $-200\text{m}$ ,  $-500\text{m}$ ,  $-1000\text{m}$ ,  $-2000\text{m}$  and the  $-3000\text{m}$  isobaths respectively.

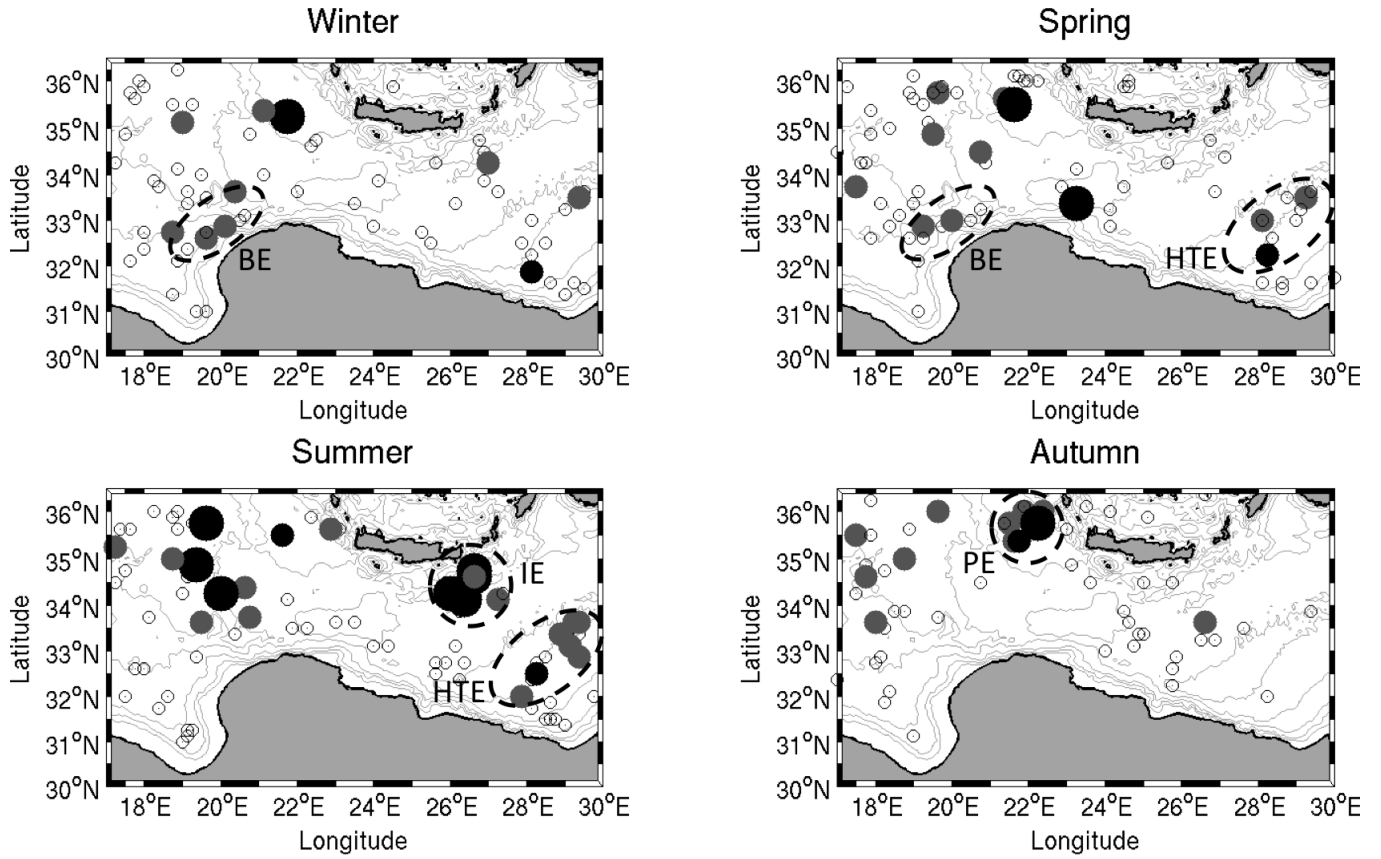


**Figure 12.** First detection points of long-lived anticyclones for the four seasons: winter (a), spring (b), summer (c) and autumn (d). The dot sizes and colors correspond to the eddy lifetime :  $\tau_L = 2 - 6$  months (open circle),  $\tau_L = 6 - 12$  months (small grey circle),  $\tau_L = 12 - 18$  months (small black circle), more than 18 months (big black dots). The grey lines represent the  $-200\text{m}$ ,  $-500\text{m}$ ,  $-1000\text{m}$ ,  $-2000\text{m}$  and the  $-3000\text{m}$  isobaths respectively. Dashed contours indicates possible formation area.

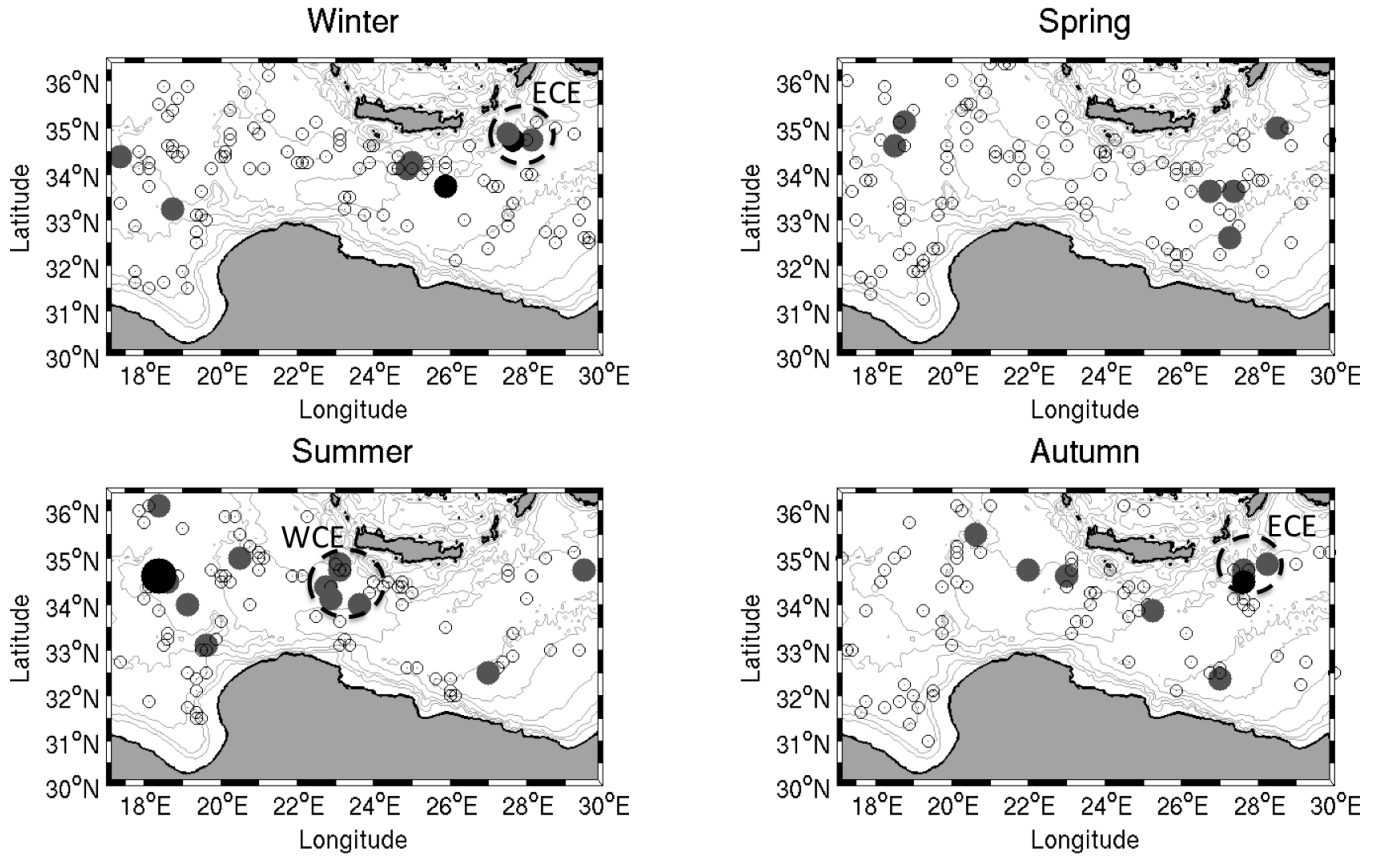


**Figure 13.** First detection points of long-lived cyclones for the four seasons: winter (a), spring (b), summer (c) and autumn (d). The dot sizes and colors correspond to the eddy lifetime :  $\tau_L = 2 - 6$  months (open circle),  $\tau_L = 6 - 12$  months (small grey circle),  $\tau_L = 12 - 18$  months (small black circle), more than 18 months (big black dots). The grey lines represent the  $-200\text{m}$ ,  $-500\text{m}$ ,  $-1000\text{m}$ ,  $-2000\text{m}$  and the  $-3000\text{m}$  isobaths respectively. Dashed contours indicates possible formation area.

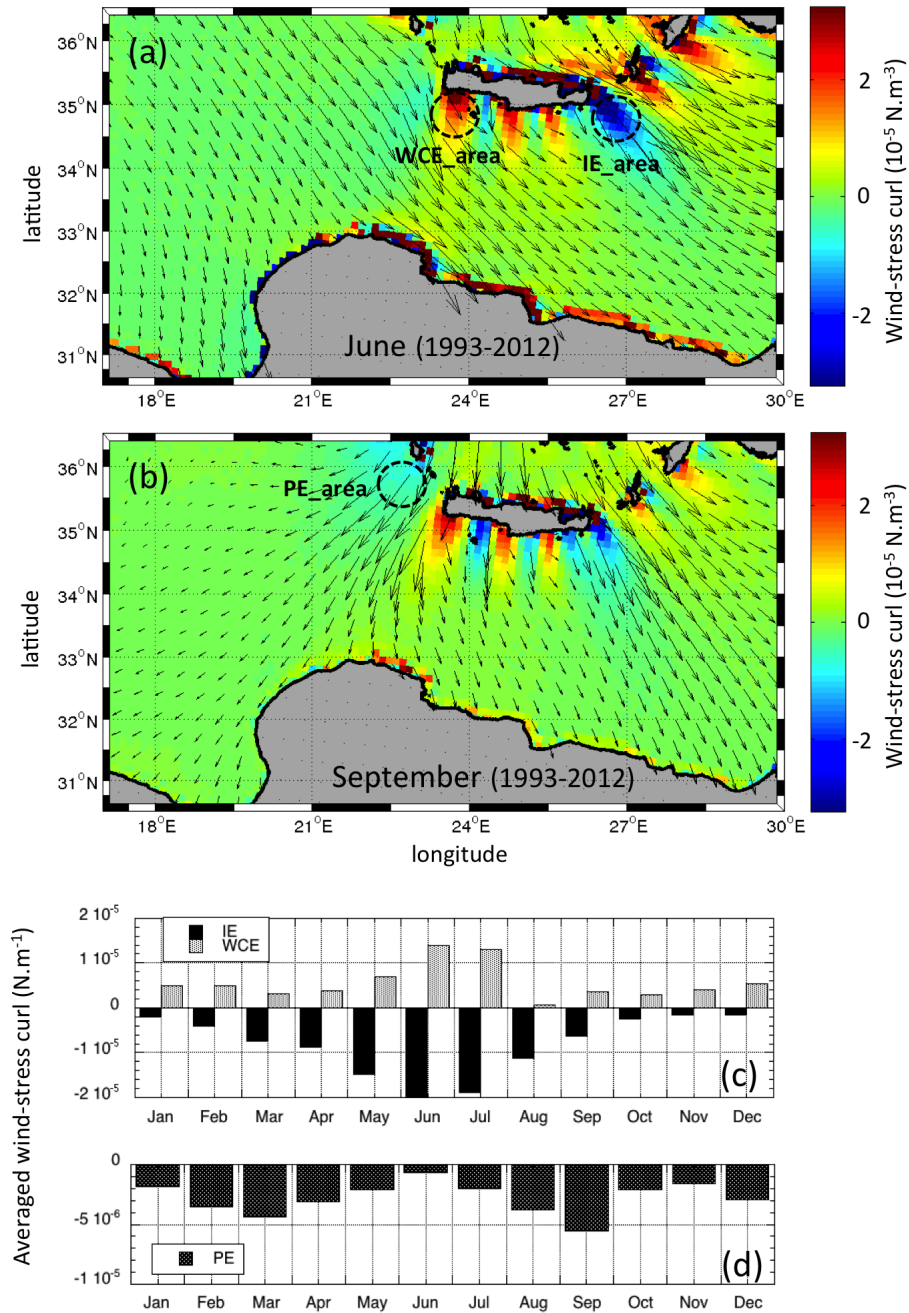


**Figure 14.** Wind-stress (black arrows) and wind stress-curl amplitude (colors) for the climatologic month of June (a) and September (b). These climatologic data are averaged during the whole month for the twenty years period (1993 – 2012). Three areas (dashed circles labeled IE\_area, PE\_area and WCE\_area) were selected for the coincidence of a strong wind-stress curl with recurrent eddy formation. The seasonal cycles of the mean amplitude of the wind-stress curl, spatially averaged in each area, are plotted in (c) and (d). Note: the high pixels values visible along the coastlines are due to systematic derivative errors between the sea and the land gridded data.

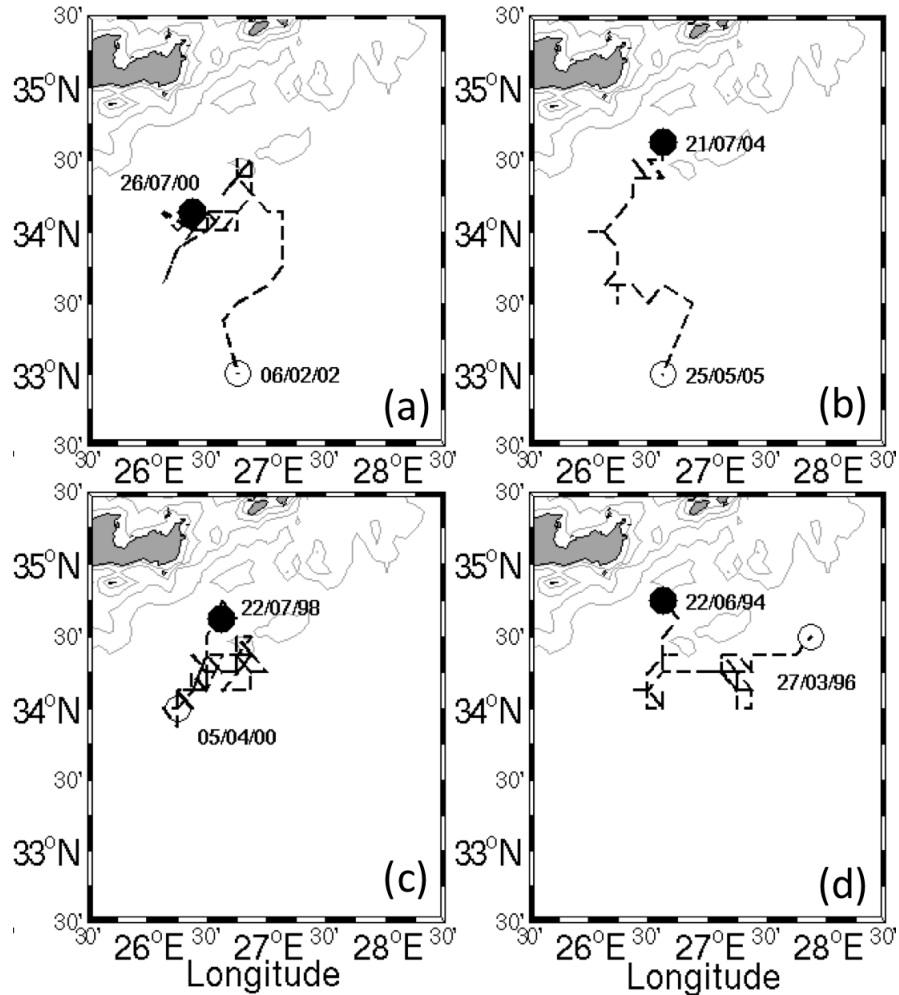


**Figure 15.** Trajectories of *long-lived* Ierapetra anticyclones (IE). The eddy trajectories (dashed lines) are plotted from the first detection point (filled circle) to the last detection point (open circle). The thin grey lines represent the  $-200\text{m}$ ,  $-500\text{m}$ ,  $-1000\text{m}$ ,  $-2000\text{m}$  and the  $-3000\text{m}$  isobaths respectively.

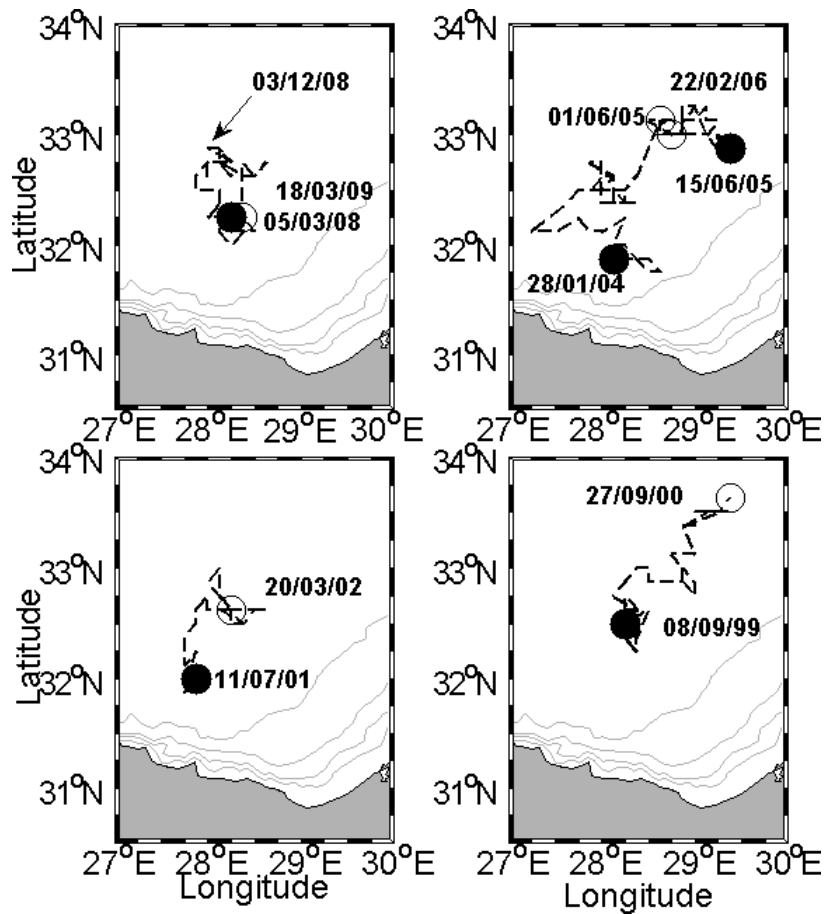


**Figure 16.** Trajectories of *long-lived* anticyclones along the Herodotus Trough. The eddy trajectories (dashed lines) are plotted from the first detection point (filled circle) to the last detection point (open circle). We add on panel (b) the “second trajectory” of the same HTE anticyclone after a strong stretching of the structure which occurs from the first to the 15 of June 2005. The thin grey lines represent the  $-200\text{m}$ ,  $-500\text{m}$ ,  $-1000\text{m}$  and the  $-2000\text{m}$  isobaths respectively.

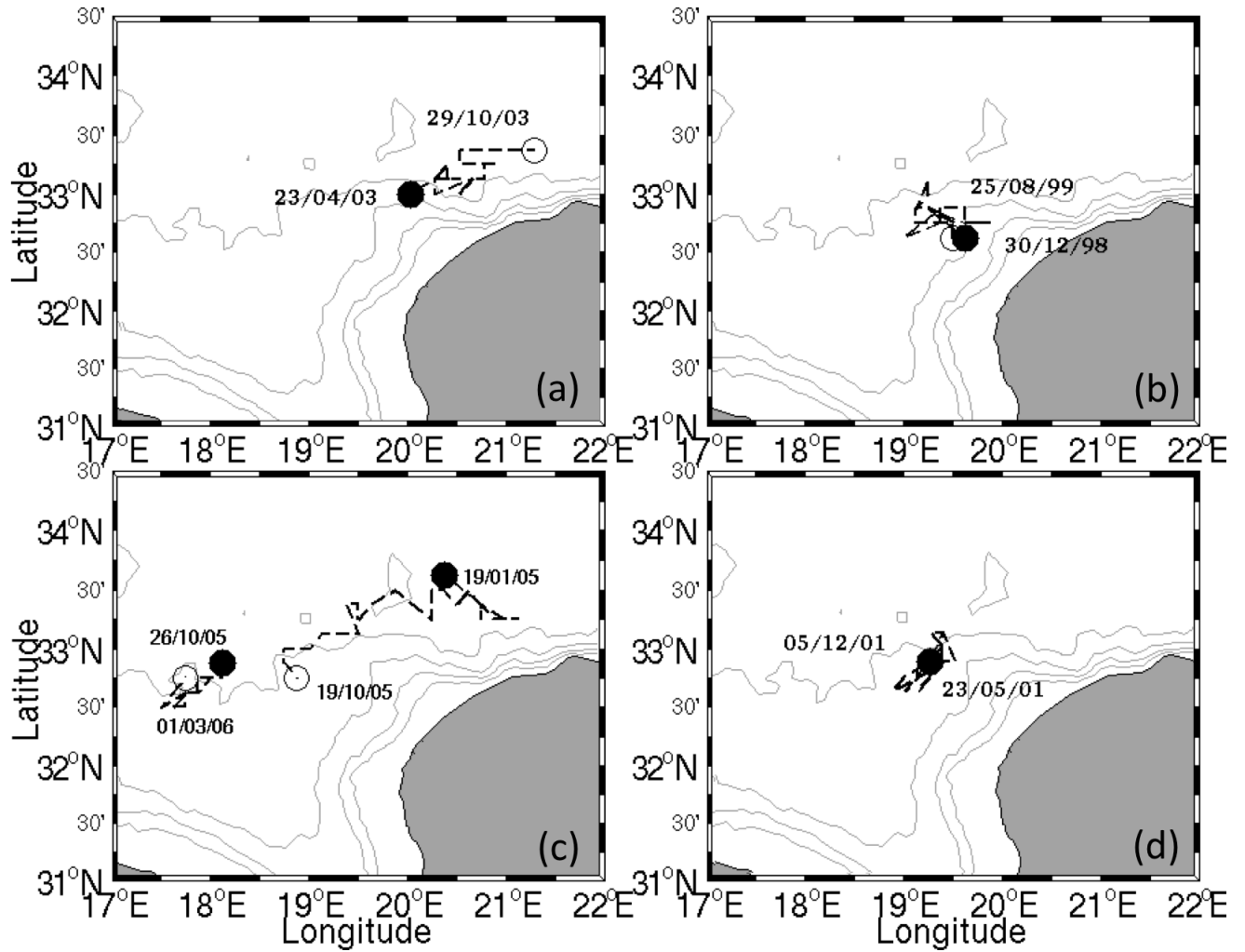


**Figure 17.** Trajectories of *long-lived* anticyclonic BE detached from the Benghazi coast. The eddy trajectories (dashed lines) are plotted from the first detection point (filled circle) to the last detection point (open circle). We add on panel (c) the “second trajectory” of the same BE anticyclone after a strong stretching of the structure which occurs from October 19<sup>th</sup> to 26<sup>th</sup> 2005. The thin grey lines represent the  $-200$  m,  $-500$  m,  $-1000$  m and the  $-2000$  m isobaths respectively.

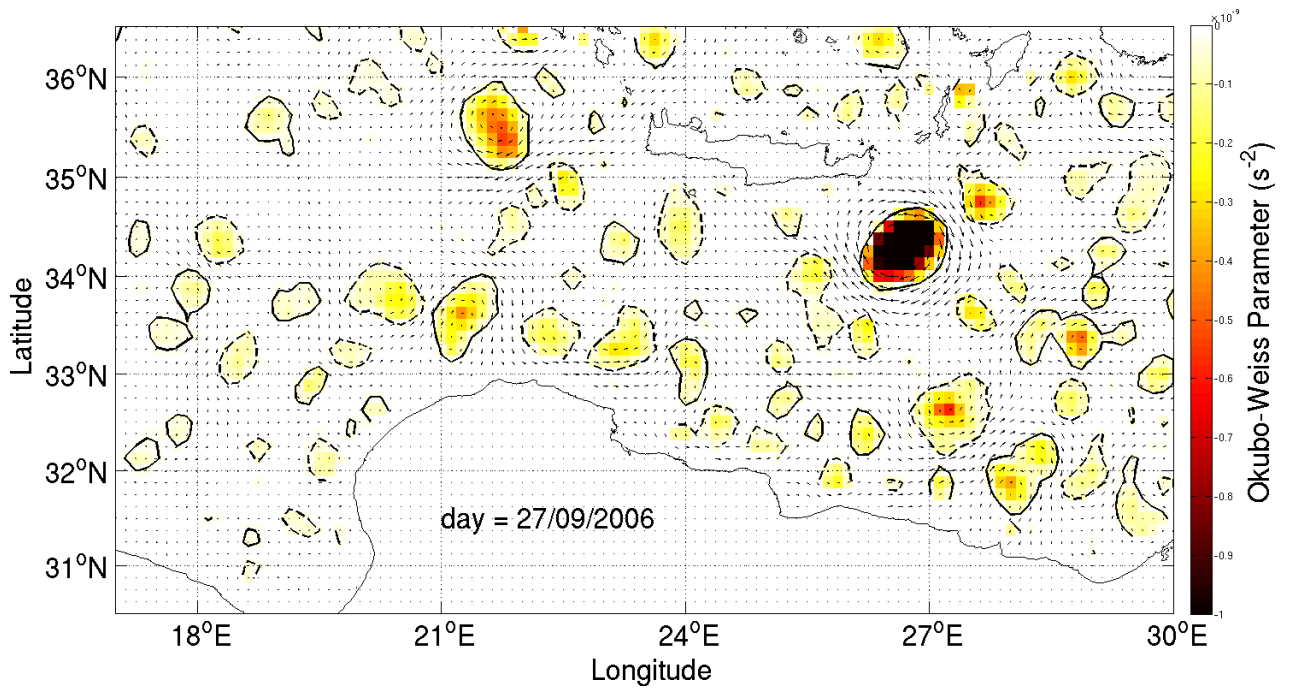


**Figure 18.** Same velocity field as in figure 3. The black solid (dashed) lines correspond to the  $W_0 = -0.2\sigma_\omega$  threshold of the Okubo-Weiss field around anticyclonic (cyclonic) core vortices.

	Surface drifters	AVISO	CTD transects
<b>LE1 anticyclone</b>			
$R_{max}$ (km)	35 – 45	28 – 32	35
$V_{max}$ (cm/s)	45	16 – 28	35 – 45
$Ro$	0.12	0.06 – 0.14	0.12
<b>IE05 anticyclone</b>			
$R_{max}$ (km)	25 – 35	35	30
$V_{max}$ (cm/s)	35	20 – 30	35 – 45
$Ro$	0.13	0.07 – 0.11	0.15

**Table 1.** Characteristics of the Libyo-Egyptian (LE1) and the Ierapetra (IE05) eddies. The characteristic radius  $R_{max}$ , the maximal tangential velocity  $V_{max}$  and the vortex Rossby numbers of the LE1 and the IE05 eddies are deduced from surface drifters measurements (drogued at 15m), CTD geostrophic currents section (April 19 to 21 2006) and the automated eddy detection applied to the AVISO ADT geostrophic velocities.